iScience

CellPress

Article

Completely Solvent-free Protocols to Access Phase-Pure, Metastable Metal Halide Perovskites and Functional Photodetectors from the Precursor Salts

Zonghan Hong, Davin Tan, Rohit Abraham John, ..., Nripan Mathews, Felipe García, Han Sen Soo

nripan@ntu.edu.sg (N.M.)
fgarcia@ntu.edu.sg (F.G.)
hansen@ntu.edu.sg (H.S.S.)

HIGHLIGHTS

Mechanochemistry provided a solvent-free perovskite and device fabrication process

Direct access to metastable phases of perovskites without post-synthetic annealing

Energy- and time-efficient synthetic protocol demonstrated up to kilogram scales

Procedures applicable for lead-based, air-sensitive tin(II), and other perovskites

Hong et al., iScience *16*, 312–325
June 28, 2019
https://doi.org/10.1016/j.isci.2019.05.042

iScience

CellPress

Article

Completely Solvent-free Protocols to Access Phase-Pure, Metastable Metal Halide Perovskites and Functional Photodetectors from the Precursor Salts

Zonghan Hong,[1] Davin Tan,[1] Rohit Abraham John,[2] Yong Kang Eugene Tay,[3] Yan King Terence Ho,[1] Xin Zhao,[1] Tze Chien Sum,[3] Nripan Mathews,[2,4,*] Felipe García,[1,*] and Han Sen Soo[1,5,6,*]

SUMMARY

Mechanochemistry is a green, solid-state, re-emerging synthetic technique that can rapidly form complex molecules and materials without exogenous heat or solvent(s). Herein, we report the application of solvent-free mechanochemical ball milling for the synthesis of metal halide perovskites, to overcome problems with solution-based syntheses. We prepared phase-pure, air-sensitive $CsSnX_3$ (X = I, Br, Cl) and its mixed halide perovskites by mechanochemistry for the first time by reactions between cesium and tin(II) halides. Notably, we report the sole examples where metastable, high-temperature phases like cubic $CsSnCl_3$, cubic $CsPbI_3$, and trigonal $FAPbI_3$ were accessible at ambient temperatures and pressures without post-synthetic processing. The perovskites can be prepared up to "kilogram scales." Lead-free, all-inorganic photodetector devices were fabricated using the mechanosynthesized $CsSnBr_{1.5}Cl_{1.5}$ under solvent-free conditions and showed 10-fold differences between on-off currents. We highlight an essentially solvent-free, general approach to synthesize metastable compounds and fabricate photodetectors from commercially available precursors.

INTRODUCTION

Metal halide perovskites have emerged as leading cost-effective candidates for light harvesting materials in commercialized solar panels over the past decade. The power conversion efficiency (PCE) of perovskite solar cells was first reported to be a modest, respectable 3.8% in 2009 (Kojima et al., 2009), but has since risen meteorically to exceed 22% in 2017 (Yang et al., 2017), potentially rivaling the performance of much more established semiconductor materials such as silicon, cadmium telluride, and gallium arsenide in the foreseeable future (Correa-Baena et al., 2017). Among the perovskites, the three-dimensional (3D) methylammonium lead iodide ($MAPbI_3$) and formadinium lead iodide ($FAPbI_3$) have been the most outstanding archetypes to achieve the recent record PCEs in photovoltaics (Bi et al., 2015; McMeekin et al., 2016; Yang et al., 2015b; Zhou et al., 2014). Furthermore, besides photovoltaics, metal halide perovskites have now been deployed in numerous optoelectronic applications including photodetectors (Deng et al., 2015; Liu et al., 2016; Su et al., 2015; Wang et al., 2015), lasers (Xing et al., 2014; Zhu et al., 2015), light-emitting diodes (Dohner et al., 2014; Tan et al., 2014; Yantara et al., 2015), and non-linear optics (Zhang et al., 2016). Although their optoelectronic properties have been remarkable, the 3D perovskites $MAPbI_3$ and $FAPbI_3$ possess several undesirable features that hinder their use in consumer products. For one, the perovskites containing organic ammonium cations MA and even FA are notoriously vulnerable to thermal (Dualeh et al., 2014; Leong et al., 2016; Noel et al., 2014) and moisture (Leguy et al., 2015; Yang et al., 2015a) degradation due to loss of their organic cations, whereas the all-inorganic $CsPbI_3$ suffers from poor phase stability. Moreover, the phase purity and crystallinity of the products are sensitive to the solvents used and the synthetic procedures. For instance, the syntheses often involve dissolving the precursors in solvents such as *N*,*N*-dimethylformamide (DMF) and then spin-coating, spray-coating, or dropcasting the solutions onto substrates, resulting in thin perovskite films. In many cases, these films are then annealed at high temperatures, enabling polymorphic transformation to the desired perovskite phases. Such solution-based processes typically show reproducibility and scalability issues beyond small devices.

Mechanochemistry is an established but re-emerging, more eco-friendly, alternative solid-state synthetic technique that can be used to rapidly synthesize small molecules and materials (Heinicke, 1984; Senna, 1993; Tkáčová, 1989). Much of the seminal work on some of the applications has been reviewed previously

[1]Division of Chemistry and Biological Chemistry, School of Physical and Mathematical Sciences, Nanyang Technological University, 21 Nanyang Link, Singapore 637371, Singapore

[2]School of Materials Science and Engineering, Nanyang Technological University, 50 Nanyang Avenue, Singapore 639798, Singapore

[3]Division of Physics and Applied Physics, School of Physical and Mathematical Sciences, Nanyang Technological University, 21 Nanyang Link, Singapore 637371, Singapore

[4]Energy Research Institute @NTU (ERI@N), Research Techno Plaza, X-Frontier Block, Level 5, 50 Nanyang Drive, Singapore 637553, Singapore

[5]Solar Fuels Laboratory, Nanyang Technological University, 50 Nanyang Avenue, Singapore 639798, Singapore

[6]Lead Contact

*Correspondence: nripan@ntu.edu.sg (N.M.), fgarcia@ntu.edu.sg (F.G.), hansen@ntu.edu.sg (H.S.S.)

https://doi.org/10.1016/j.isci.2019.05.042

Current State-of-the-Art for Mechanochemical Synthesis of Metal Halide Perovskites	This Article's Innovations
1. Predominantly air-stable, highly toxic, Pb-based perovskites were prepared	1. First examples of the oxidatively unstable, less-toxic, Sn-based perovskites demonstrated, together with Pb-based examples to illustrate versatility
2. Milligram- to gram-scale syntheses	2. Industrially relevant "kilogram scale"
3. Mainly room-temperature-stable perovskite phases demonstrated	3. First three examples of metastable perovskite phases of cubic $CsSnCl_3$, cubic $CsPbI_3$, and trigonal $FAPbI_3$ accessed under ambient temperature and pressure
4. Metastable perovskite phases accessed by addition of additives or post-synthetic annealing (Askar et al., 2018; El Ajjouri et al., 2018b; Prochowicz et al., 2017)	4. No post-synthetic annealing or other processing and no additives or surfactants required to access phase-pure metastable forms
5. Post-synthetic, solvent-based perovskite device fabrication (Prochowicz et al., 2017, 2018)	5. Unprecedented, greener, low-cost, solvent-free perovskite photodetector fabrication from precursor salts
6. Perovskite photodetectors containing Pb or thermally unstable MA cations (Fang et al., 2019; Ji et al., 2018; Waleed et al., 2017; Wang et al., 2019; Yang et al., 2018)	6. Greener, Pb-free, all-inorganic perovskite photodetector

Table 1. Comparison between Existing Technologies and Our Protocols
See also Table S1.

(Avvakumov et al., 2001; Baláž, 2008; Balaz et al., 2013; Boldyrev, 2006; Boldyrev and Tkáčová, 2000; Boldyreva, 2013; Jones and Eddleston, 2014; Takacs, 2002). Recently, mechanochemistry has efficiently and reproducibly provided access to metastable products in solvent-free environments, where traditional solution-based chemistry was unsuccessful (Do and Friscic, 2017; James et al., 2012). Modern mechanochemical reactions are performed using automated ball mills, such as shaker mills or large-scale planetary mills. The reaction vessel is charged with ball bearings, typically made of hardened stainless steel, and is oscillated or spun at a controlled speed. Such solid-state milling circumvents the need to find suitable solvents and enables access to compounds that were unattainable using solution-based methodologies (Hernandez and Bolm, 2017).

Moreover, mechanochemistry has been successfully applied for the kilogram-scale synthesis of products such as metal-organic frameworks (MOFs) (Crawford et al., 2015). Although mechanochemistry had mainly been used in the preparations of pharmaceutical cocrystals and inorganic alloys and oxides (James et al., 2012), seminal studies by several groups have demonstrated its compatibility for the synthesis of a few lead halide perovskites (Jana et al., 2017; Jodlowski et al., 2016; Karmakar et al., 2018; Manukyan et al., 2016; Muñoz-Batista et al., 2018; Pal et al., 2018; Prochowicz et al., 2015; Stoumpos et al., 2013; Zhu et al., 2017). However, these examples focused on known, room-temperature, phase-stable, lead-based perovskites obtained in small scales (Askar et al., 2018; El Ajjouri et al., 2018a, 2018b; Jana et al., 2017; Pal et al., 2018; Posudievsky et al., 2017; Prochowicz et al., 2017, 2018; Protesescu et al., 2018; Rosales et al., 2019; Sadhukhan et al., 2018; Yun et al., 2018). Meanwhile, mechanochemistry in air-sensitive syntheses remains underexplored, which is crucial for perovskite materials. Furthermore, some perovskites such as $FAPbI_3$ in its black trigonal phase, which are technologically relevant for solar cells and optoelectronic devices, have previously not been accessible in their metastable phase at room temperature other than in nanocrystalline form, with added additives, or after post-synthetic annealing. Among these reports, there were only two reported device applications and both were about solar cells (Prochowicz et al., 2017, 2018). Critically, the subsequent device fabrication involved solution processing, which could transform the initial, desired metastable perovskite into other phases and diminished the impact of the solvent-free synthesis (Prochowicz et al., 2017, 2018). We envision employing mechanochemistry to achieve a completely solvent-free process for the fabrication of perovskite devices. Tables 1 and S1 highlight our current article's sustainable and significant advances when compared with previously reported studies.

As part of the sustainable energy and green chemistry efforts in our team, we have recently been developing multi-dimensional lead and tin halide perovskites for light absorption and emission purposes (Koh et al., 2016; Thirumal et al., 2017) and creating innovative energy solutions based on artificial photosynthesis (Dokic and Soo, 2018; Gazi et al., 2017; Hong et al., 2019; Lim et al., 2018; Ng et al., 2018). Simultaneously, we have also been developing more eco-friendly, essentially solvent-free, mechanochemical approaches for the synthesis, functionalization, and transformation of main group compounds (Shi et al., 2016; Sim et al., 2017, 2018) and complexes (Geciauskaite and Garcia, 2017; Tan and Garcia,

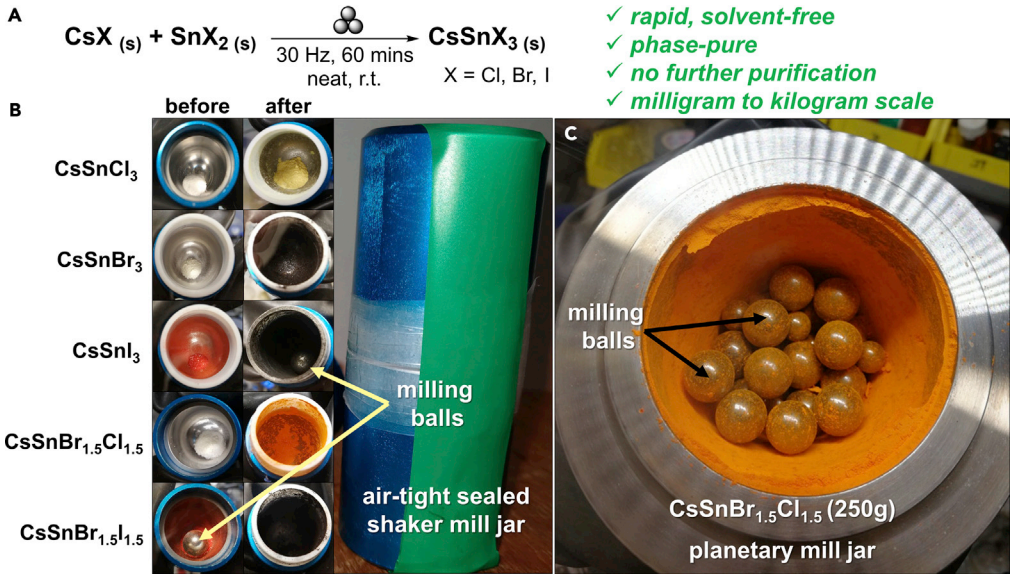

Figure 1. Mechanochemical Synthesis of All-Inorganic Tin Halide Perovskites.

(A) Reaction scheme for the ball milling reaction to form all-inorganic tin perovskites using CsX and SnX_2 (X = Cl, Br, I). The three-ball symbol above the arrow represents the mechanochemical procedure. The powders were prepared in a N_2-filled glove box, sealed in air-tight vessels, and then milled for 60 min. The key advantages of performing such mechanochemical ball milling synthesis are highlighted in green.

(B) Photographs depicting the reagents before and after milling on 200-mg scales.

(C) Photograph of a 250-g scale reaction of the mixed halide perovskite $CsSnBr_{1.5}Cl_{1.5}$ after 10 h of milling.

See also Figures S1–S3 and S13.

2019; Wang et al., 2016, 2017). In a joint endeavor, we sought to use mechanochemistry to address the challenges encountered in solution-based syntheses of purportedly unstable metal halide perovskites.

Herein, we present the solvent-free preparation of phase-pure, all-inorganic $CsSnX_3$ (X = I, Br, Cl) perovskites by ball milling cesium and tin(II) halide salts. The successful syntheses of these air-sensitive perovskites underscore the advantages of mechanochemistry over current solution-based syntheses. Furthermore, $FAPbI_3$ and $CsPbI_3$ perovskites in their high-temperature stable phases were also prepared at room temperature to emphasize the generality of our approach. Notably, we demonstrate that the powdered products can be converted into effective photodetectors, which is an unprecedented instance of entirely solvent-free perovskite device fabrication from the precursor salts. This report illustrates how we used unconventional, low-energy synthetic protocols to synthesize perovskites and also fabricate functional perovskite devices in practical scales under environmentally benign, virtually solvent-free conditions.

RESULTS AND DISCUSSION

Versatile Access to Oxidatively Unstable Sn Halide Perovskites under Ambient Temperatures and Pressures

Reasonably high-purity (at least 99%) precursor salts were purchased for the syntheses, and all the new bottles of precursors and the derived products were handled exclusively in a glove box (Figure S1 and Table S2, see Transparent Methods in Supplemental Information for details). As a preliminary reaction on a 200-mg scale, CsI and SnI_2 were placed in a 10-mL stainless-steel jar with a 1:1 stoichiometric ratio, along with one 10-mm 4.0-g stainless-steel ball providing a ball-to-reagent ratio (BRR) of 20 (Figure 1A). The reaction was set up in a N_2 glove box to prevent the oxidation of Sn(II) to Sn(IV), sealed and removed from the glove box, and subsequently placed in a vibration mill. After 60 min of oscillation at 30 Hz, the solids were collected from the reaction vessel in a glove box, without annealing or further purification, and the uniformly colored product (Figure 1B) was characterized using powder X-ray diffraction (PXRD) in an airtight specimen holder. As shown in Figures 2A–2G, the PXRD pattern of the product matched perfectly with that of the previously reported black orthorhombic polymorph of $CsSnI_3$ perovskite and a

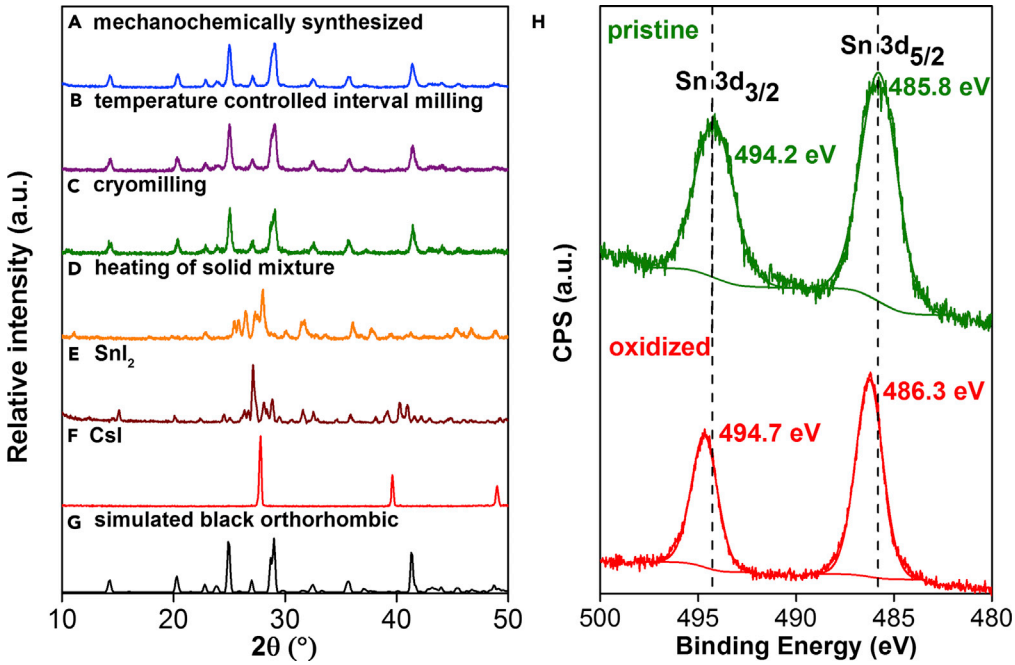

Figure 2. Comparison of Data for Mechanochemically Synthesized $CsSnI_3$ with those from Control Experiments.
(A–F) Comparison of the PXRD patterns of $CsSnI_3$ perovskite synthesized by (A) mechanochemical ball milling, (B) temperature-controlled interval milling, (C) cryomilling under liquid N_2, and (D) heating of the solid reagents in a sand bath up to 320°C under Ar. For reference, the PXRD patterns of the starting materials (E) SnI_2 and (F) CsI are shown.
(G) Simulation of the black, orthorhombic phase of $CsSnI_3$ based on single-crystal XRD data.
(H) Comparison of the XPS data of the pristine, mechanochemically synthesized $CsSnI_3$ perovskite (green) and the oxidized sample upon exposure to air for 30 min (red).
See also Figures S4–S7 and S19.

simulation from single-crystal data, and did not show any other impurities. Such phase purity for $CsSnI_3$ is in stark contrast with prior solution-based methods (Konstantakou and Stergiopoulos, 2017).

To eliminate the possibility of frictional heat-induced reactivity during milling, several temperature-controlled experiments were performed. These include (1) milling at cryogenic temperatures using liquid N_2; (2) milling for 5 min, with 10-min cooling intervals (total milling duration remained at 60 min), with the temperature maintained around 27.5°C, as monitored via an infrared thermometer; and (3) heating of the solid mixture at 320°C under Ar (Figures S4–S6). The PXRD patterns of the interval milling and cryomilling experiments matched those of the desired black orthorhombic phase $CsSnI_3$ (Figure 2). Conversely, thermal heating of the premixed solid precursors at 320°C (the melting point of SnI_2) in a sealed flask under an inert Ar atmosphere resulted in the formation of the yellow orthorhombic phase, along with unreacted CsI. These results indicate that mechanochemical treatment is essential for the observed chemical reactivity, and product formation is not merely induced by frictional heat produced during milling.

Subsequently, we verified the oxidation state of Sn in the mechanochemically synthesized $CsSnI_3$ perovskite with X-ray photoelectron spectroscopic (XPS) studies (Figure 2H). The XPS experiments were all conducted under high vacuum at ambient temperatures between 295 and 298 K (see Supplemental Information for details). The measured binding energies of the $3d_{3/2}$ and $3d_{5/2}$ electrons suggested that the Sn existed as a single-oxidation-state species. Upon exposure to air for 30 min, an approximate 0.5-eV increase in the binding energies was observed, which corresponded to the formation of Sn(IV) due to oxidation. In addition, the XPS survey spectra (Figures S7–S11) showed no signals from any Fe species (Fe 3s and 3p electrons), which could have resulted from wear of the milling media, i.e., the balls and the jar. The XPS data confirm the phase and composition purity because metal contaminants from the milling media can affect the overall composition and properties of the perovskite (Granger et al., 2016).

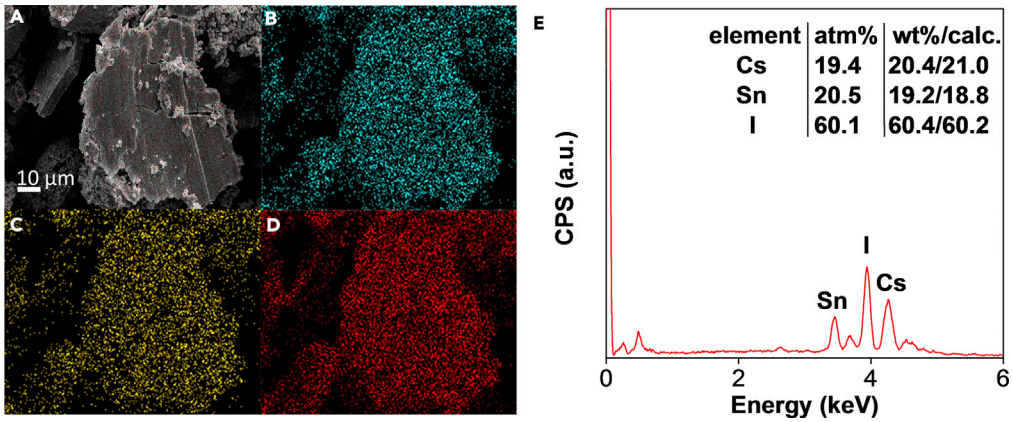

Figure 3. SEM and EDX Data of Mechanochemically Synthesized $CsSnI_3$

(A–D) (A) SEM image of the mechanochemically synthesized $CsSnI_3$ perovskite, with EDX analysis of the different elements (B) Cs (blue), (C) Sn (yellow), and (D) I (red), illustrating that the elements are homogeneously distributed throughout the solid particles.

(E) The elemental composition as determined by EDX shows an approximately 1:1:3 molar ratio of Cs:Sn:I atoms, which coincides with the chemical formula of $CsSnI_3$. The experimental weight percentages of each element showed no significant deviation from the calculated values.

See also Figures S7 and S19.

Besides X-ray diffraction and photoelectron spectroscopic characterization, scanning electron microscopy (SEM) coupled with energy dispersive X-ray (EDX) was employed (Figure 3) to confirm that the $CsSnI_3$ solid produced is a homogeneous and pure phase. The SEM studies revealed that the mechanochemically synthesized powder is composed of micron-sized particles, and elemental mapping showed that it is indeed a homogeneous phase (Figures 3A–3D). Moreover, the elemental composition of the product by weight percentage (wt %) and atomic percentage (atm %) derived from EDX corroborates with the $CsSnI_3$ perovskite formula (Figure 3E).

The successful, efficient, and rapid formation of phase-pure $CsSnI_3$ encouraged us to expand our mechanochemical protocol to other halide precursors (Figure 1B) and obtain the corresponding $CsSnX_3$ (X = Cl, Br). The desired perovskites were readily produced in their cubic phases, as evidenced by the PXRD data, without further optimization. The cubic polymorphs of the $CsSnX_3$ perovskites are all isostructural with only minor shifts in the relative peak positions of their PXRD patterns and can be readily distinguished from one another (Figure 4). Furthermore, we investigated the formation of mixed halide perovskites such as $CsSnBr_{1.5}Cl_{1.5}$ and $CsSnBr_{1.5}I_{1.5}$, which were readily obtained using our mechanochemical method. Notably, these mixed halide perovskites are produced with precise stoichiometric control, and they consist of phase-pure mixed halides rather than a mixture of their constituent single-halide perovskites, as evidenced by PXRD analysis (Figure 4) and SEM-EDX studies (Figure S12). This highlights a major advantage of mechanochemistry over solution-based processes. For solution-based methods, the stoichiometric outcome of the product can depend on the precursor solubility, temperature, and other reaction conditions, which can affect the recrystallization rates and thus the final composition of the material (Zhu et al., 2017). In addition, instances of solvent-free, neat, mechanochemical reactions facilitating the formation of cubic-phased perovskites are rare (Jana et al., 2017).

Industrially Relevant "Kilogram-Scale" Syntheses of Perovskites

The scalability of the mechanochemical solid-solid reaction was then investigated with a planetary ball mill containing four 250-mL reaction vessels. We first attempted a 25-g (50 mmol scale) synthesis of $CsSnBr_3$ by neat milling CsBr and $SnBr_2$ for 3 h, using one 250-mL reaction vessel charged with a mixture of 4.0-g and 13.5-g stainless-steel milling balls (BRR = 2.35, Figure S2). Remarkably, full conversion of the precursors occurred as confirmed by PXRD measurements (Figure 4). We isolated 23.55 g of the pure, black, cubic-phase $CsSnBr_3$ in the glove box, which corresponded to a 94% yield. It is noteworthy that this scale-up from 200 mg in a shaker mill to 25 g in a planetary ball mill did not require much optimization, apart from increasing the reaction time and varying the BRR.

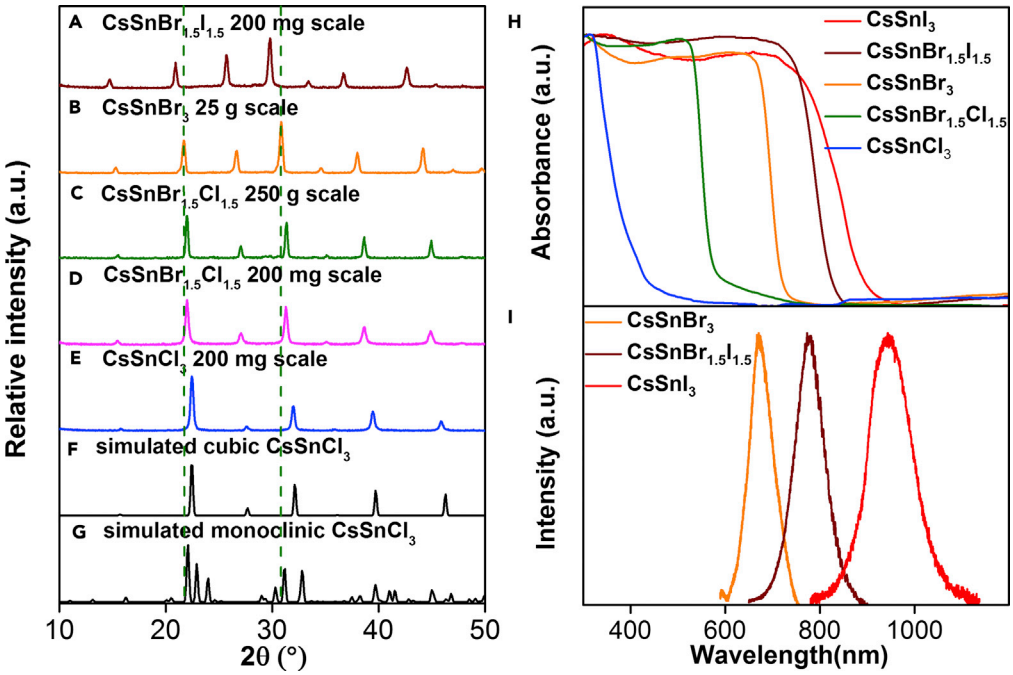

Figure 4. PXRD and Optical Characterization of Mechanochemically Synthesized Tin Halide Perovskites

(A–H) Comparison of the PXRD patterns of the mechanochemically synthesized (A) 200-mg-scale $CsSnBr_{1.5}I_{1.5}$, (B) 25-g-scale $CsSnBr_3$, (C) 250-g-scale $CsSnBr_{1.5}Cl_{1.5}$, (D) 200-mg-scale $CsSnBr_{1.5}Cl_{1.5}$, and (E) 200-mg-scale $CsSnCl_3$ perovskites with the simulated (F) cubic and (G) monoclinic phases of $CsSnCl_3$. The green dashed lines help to show that the various $CsSnX_3$ perovskites are distinct but isostructural to one another, and that they all correspond to the cubic polymorph. These scalable mechanochemical reactions clearly contain phase-pure cubic products. The (H) UV-vis DRS spectra and (I) PL spectra of the various mechanochemically synthesized perovskites. The PL of the $CsSnCl_3$ perovskite was measured but was not detectable. See also Figures S8–S14.

Encouraged by these results, we then performed the mechanochemical synthesis of the mixed halide $CsSnBr_{1.5}Cl_{1.5}$ on a 250-g scale, using the same 250-mL reaction vessel, as a proof of concept to access perovskites in "kilogram scales." A powdered mixture of CsBr, CsCl, $SnBr_2$, and $SnCl_2$ (0.29 mol each) was added to the reaction vessel in a N_2 glove box and charged with stainless-steel balls (BRR = 1.30). The air-tight vessel was then installed in a planetary mill, and the reagents were milled for a total of 10 h (Figure S3, see Supplemental Information for details). The milling time was increased to ensure complete conversion. A bright orange solid powder (240.9 g, 96% isolated yield) was obtained (Figure 1C). Full utilization of all four vessel holders of the planetary mill would thus enable the solvent-free synthesis of around 1 kg of the desired perovskite. PXRD analysis confirmed the absence of all the four precursors, and the pattern was indistinguishable from pure, metastable cubic $CsSnBr_{1.5}Cl_{1.5}$ (Figure S13). These large-scale experiments highlight the scalability of the mechanochemical reactions, without compromising the quality and selectivity of the products.

Subsequently, UV-visible diffuse reflectance spectroscopic (UV-vis DRS) and steady-state photoluminescence (PL) studies were conducted to evaluate the optical properties of our mechanochemically synthesized perovskites. All optical measurements were conducted at ambient temperatures and pressures on samples that had been sealed into air-tight quartz cuvettes inside a glove box before being transferred to the spectrometer (see Supplemental Information for details). The UV-vis spectra (Figure 4H) revealed that the tin halide perovskite absorbs light within the 200- to 900-nm region, similar to their lead-based counterparts (Zhu et al., 2017). The $CsSnBr_3$ and $CsSnI_3$ samples showed PL with narrow peaks at 673 and 943 nm (Figure 4I), respectively, upon excitation using a 500-nm laser source, whereas their spin-coated thin-film counterparts had very similar but broader PL peaks positioned at 674 and 941 nm, respectively (Figure S14A). Owing to the lower solubilities of CsBr and $SnBr_2$ compared with their iodide homologs in DMF, we observed that it was more difficult to obtain a uniform, spin-coated thin film of $CsSnBr_{1.5}I_{1.5}$, possibly due to the different crystallization kinetics of the disparate halide salts (bromides crystallize faster)

from DMF solutions. Consequently, the PL intensity and signal-to-noise ratio for the $CsSnBr_{1.5}I_{1.5}$ was comparatively poorer than its monohalide congener (Figure S14A). Notably, these results verify that the optical properties of the mechanochemically synthesized perovskites are from phase-pure products with improved crystallinity over their conventional solution-processed counterparts. For the mixed halide $CsSnBr_{1.5}Cl_{1.5}$ and $CsSnBr_{1.5}I_{1.5}$, their UV-vis absorption and PL maxima are between those of their single-halide counterparts, indicating the tunability of the optical properties. By simply varying the stoichiometric composition of each halide, it is possible to achieve stoichiometrically altered perovskites with the specifically desired optical absorption, which is less predictable for solution-based methods.

Unprecedented Access to Technologically Relevant Metastable Phases without Additives and Post-synthetic Thermal Annealing

For $CsSnCl_3$ to be isolated as the pure cubic phase described above is unprecedented, because the cubic polymorph is known to be a metastable high-temperature phase and was previously thought to be achievable only by heating the monoclinic phase to at least 117°C (Peedikakkandy and Bhargava, 2016; Scaife et al., 1974). The ability to prepare the cubic phase for $CsSnCl_3$ by mechanochemistry inspired us to explore the possibility of obtaining the metastable high-temperature phases for other perovskites. To establish that our ball milling methodology is highly versatile and applicable to all metal halide perovskites, we conducted the mechanochemical synthesis of two other metastable and technologically relevant perovskite phases, the hybrid inorganic-organic $FAPbI_3$ and the all-inorganic $CsPbI_3$ systems. Remarkably, unlike previous reports on accessing metastable lead halide perovskites (Askar et al., 2018; El Ajjouri et al., 2018b; Prochowicz et al., 2017), our current protocol is conducted at ambient temperature and pressure, does not require the introduction of additives or surfactants, and also does not need post-synthetic thermal annealing or other processing.

It is known that $FAPbI_3$ can exist as two polymorphs, namely, the black trigonal and the yellow hexagonal phases (Weber et al., 2018). The metastable black trigonal phase of $FAPbI_3$ was previously obtained by heating the yellow hexagonal phase to 185°C (Han et al., 2016). Similarly, for $CsPbI_3$, the metastable, non-nanocrystalline, black cubic phase was only achieved at elevated temperatures, up to 260°C, as reported recently by Pradhan et al. (Pradhan et al., 2018) In addition, it is noteworthy that such solution processing methods had either been unsuccessful in obtaining a pure high-temperature phase product for these two lead-based perovskites at room temperature, or required the use of corrosive starting reagents like hydroiodic acid or sustained heating for several days.

For the mechanochemical synthesis of $FAPbI_3$, our preliminary reaction involved ball milling FAI and PbI_2 in a shaker mill for 1 h. Despite the product's uniform black color, PXRD analysis revealed that it was composed of a mixture of the yellow hexagonal and black trigonal phases, consistent with solution-based results (Han et al., 2016). It had been previously established that mechanochemistry can be used to alter product selectivity (Hernandez and Bolm, 2017) by changing experimental parameters such as the milling frequency, duration of milling, or the BRR. The solid-state selectivity can also be enhanced by using small quantities of a liquid milling auxiliary, which serves as a lubricant to improve mixing of the reagents, also known as liquid-assisted grinding (LAG) (Friscic et al., 2006). Systematic screening of these parameters (Figure 5) revealed that the yellow hexagonal phase can be readily obtained by solvent-free milling for 10 min, whereas the pure black trigonal phase can be afforded by LAG for 15 min, using pentane as a milling auxiliary. Prolonged milling led to mixed-phase products.

It is significant that our mechanochemical protocol enabled selective access to the metastable $FAPbI_3$ at room temperature without further annealing. The rapid (10–15 min) and efficient formation of the pure individual phases by mechanochemistry further highlights its benefits over the solution-based counterparts. We observed by PXRD that impurities arising from the yellow hexagonal $FAPbI_3$ appeared with the black trigonal phase within 4 days after the mechanochemical synthesis (Figure S15). This rapid phase transition of $FAPbI_3$ underscored the remarkable phase purity and ability to reliably access metastable materials by our mechanochemical protocol. The UV-vis DRS spectrum of the $FAPbI_3$ indicated that the absorption edge is at 800 nm, with the PL maximum at 814 nm (Figure 6A), which are consistent with reported values (Han et al., 2016). Time-resolved PL (TRPL) measurements of the as-synthesized trigonal phase powder were also conducted at 130 $\mu J\ cm^{-2}$, and two decay processes were observed. The fast decay process with a 270-ps lifetime (69%) likely arises from trap-assisted recombination, whereas the slow process with 1.6 ns (31%) could originate from free charge-carrier recombination (Figure 6B).

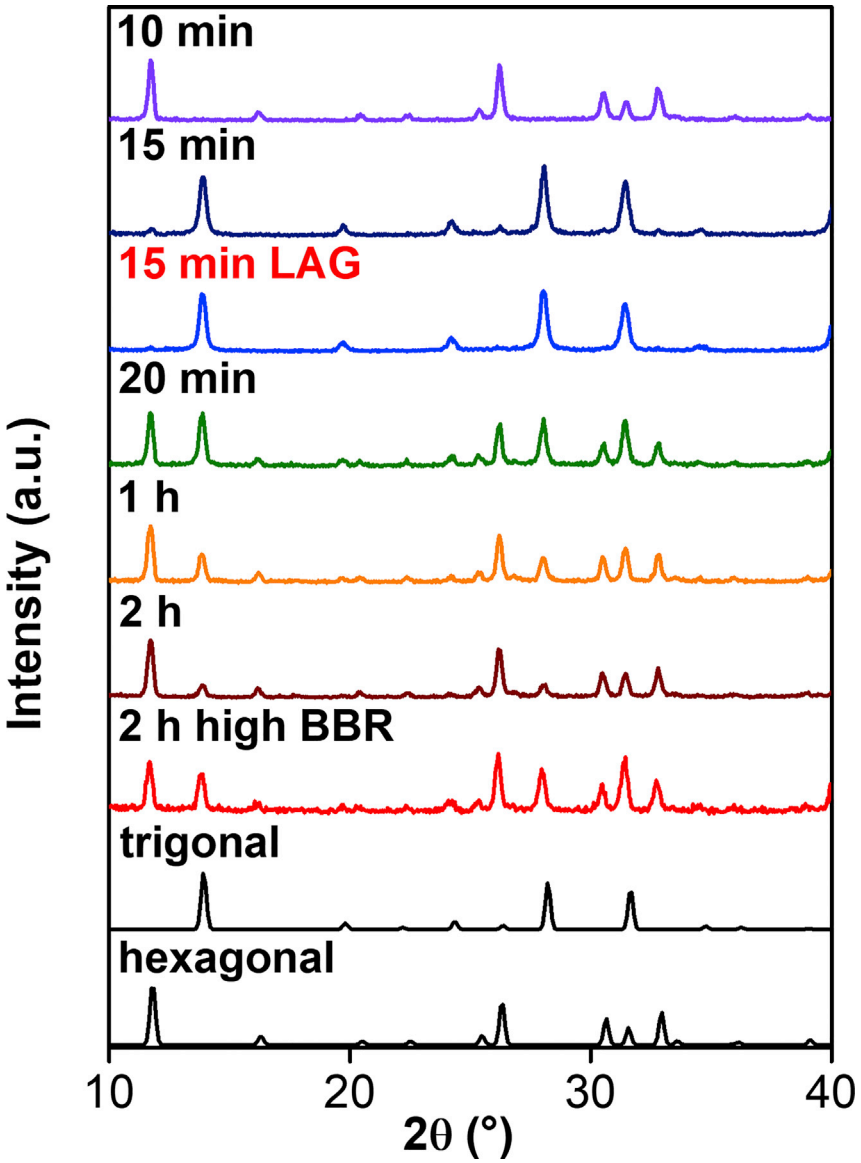

Figure 5. The PXRD Patterns for the Mechanochemically Synthesized FAPbI3 Perovskites at Different Conditions
See also Figures S15–S17.

Likewise, for the synthesis of the all-inorganic $CsPbI_3$ perovskite, our mechanochemical protocol involved ball milling of CsI and PbI_2 precursors for 15 min, which rapidly afforded the desired high-temperature black cubic phase, as confirmed by PXRD (Figure S16A). This is in stark contrast to reported solution-based protocol, which utilizes corrosive hydroiodic acids and requires additional capping reagents such as oleic acids and oleylamine as well as molten Cs-oleate precursors (Pradhan et al., 2018). *Ex situ* PXRD measurements revealed that ball milling for only 5 min resulted in the formation of a mixed black cubic and yellow orthorhombic phase product. The yellow orthorhombic phase then rapidly converts into the black cubic phase upon prolonged milling. The UV-vis absorption edge of the synthesized powder product was determined to be at 700 nm, whereas the PL maximum was centered at 724 nm (Figure S16B). TRPL measurements were also carried out at 20 μJ cm^{-2} and revealed two decay processes with lifetimes of 85 ps and 1.1 ns (Figure S16C). Especially remarkable is the prolonged stability of the $CsPbI_3$ prepared by our methods. The yellow orthorhombic $CsPbI_3$ phase was recently prepared by mechanochemical synthesis under ambient conditions, followed by thermal annealing to access the black cubic phase (Karmakar et al., 2019). The authors conducted a thorough kinetic analysis with

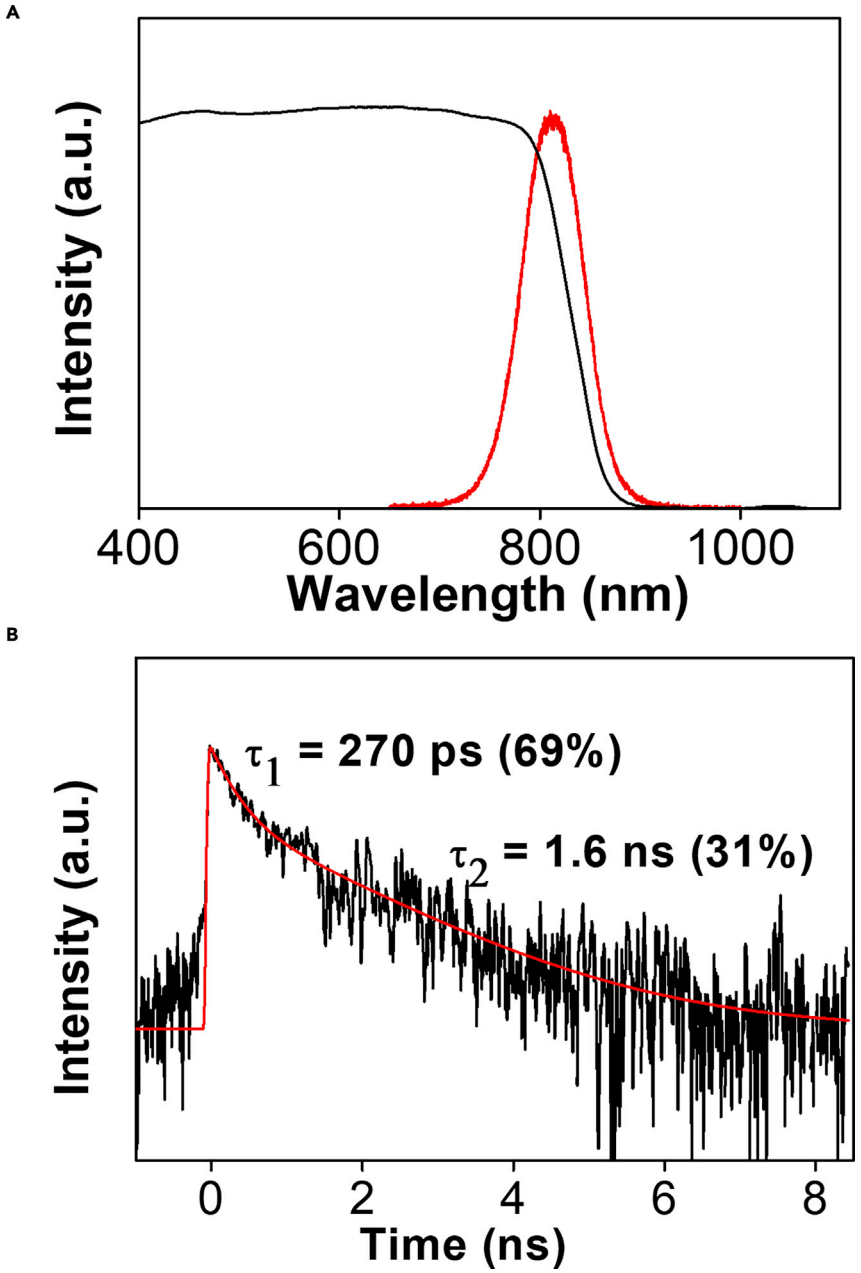

Figure 6. Steady-State and Time-Resolved Spectroscopic Data of Mechanochemically Synthesized Trigonal $FAPbI_3$.
(A) UV-vis DRS and PL measurements of the trigonal $FAPbI_3$ synthesized using our solvent-free protocol.
(B) TRPL of as-synthesized trigonal FAPbI3 upon excitation at 400 nm. The plot was fitted biexponentially to give a short-lived process with a lifetime of 270 ps and a longer process with a lifetime of 1.6 ns.
See also Figures S14, S16, and S17.

^{133}Cs solid-state nuclear magnetic resonance spectroscopy and concluded that the cubic $CsPbI_3$ has a half-life of only around 29 min under ambient atmospheric conditions (Karmakar et al., 2019). In our hands, however, we observed that $CsPbI_3$ prepared by our mechanochemical synthesis appears to remain indefinitely stable at room temperature and pressure, as long as it is stored in a glove box with <0.5 ppm of water and O_2 (Figure S17). This highlights another advantage of the versatility in using mechanochemical synthesis to access nominally air-, moisture-, or thermally sensitive metal halide perovskites or other compounds.

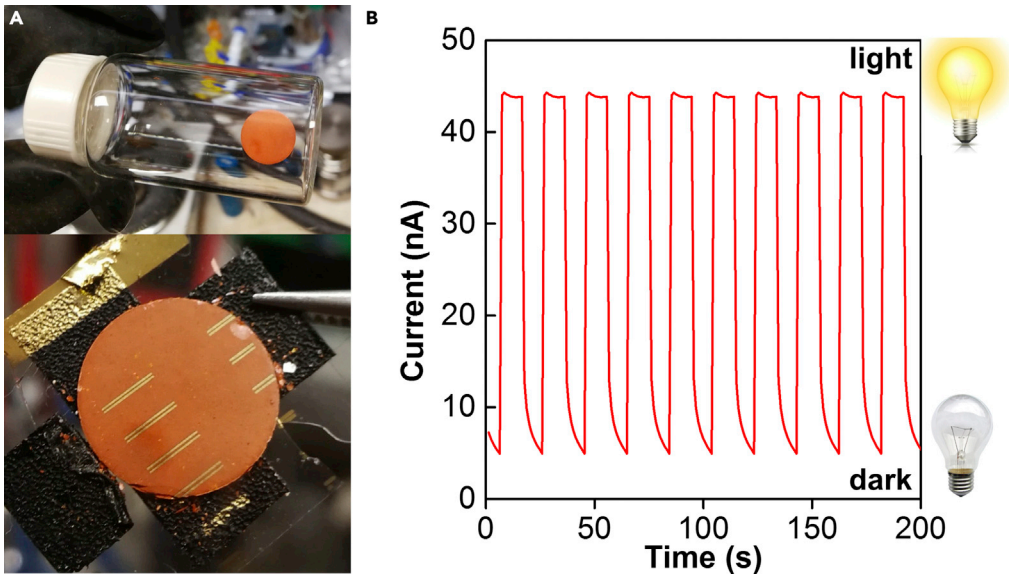

Figure 7. Photodetector Fabricated under Solvent-Free Conditions from Mechanochemically Synthesized $CsSnBr_{1.5}Cl_{1.5}$

(A) Images of the fabricated photodetector device made from mechanochemically synthesized $CsSnBr_{1.5}Cl_{1.5}$.

(B) The current versus time curve for a device made from mechanochemically synthesized $CsSnBr_{1.5}Cl_{1.5}$ with a light intensity of 0.55 mW under a bias of 0.10 V, denoting multiple light-dark cycles.

See also Figure S18.

Completely Solvent-free Fabrication of Functional, All-Inorganic Perovskite Devices from Precursor Salts

Perovskites have been widely studied for their optoelectronic properties. Despite numerous reports of lead halide perovskites for optoelectronic applications, their tin-based counterparts are plagued by undesirable dark conductivity at room temperature owing to high densities of defects, so their incorporation into devices remains challenging. Notably, all previous reports of applications from mechanochemically synthesized perovskites required post-synthetic solution processing (Prochowicz et al., 2017, 2018). In addition, only solar cells have been presented as the device application (Prochowicz et al., 2017, 2018), including one groundbreaking solvent- and vacuum-free route to perovskite solar cells, although pressure treatment instead of mechanochemistry was employed (Chen et al., 2017). Yet, it has been previously proposed that the orthorhombic black $CsSnI_3$ can be used as a promising alternative to toxic gallium arsenide (GaAs) as a semiconductor material (Tanaka, 2004; Xing et al., 2014). In addition, the cubic $CsSnBr_3$ has also shown great potential for photodetector applications (Konstantakou and Stergiopoulos, 2017).

As a proof of concept that functional devices can be made from their precursors in a completely solvent-independent manner, we fabricated photodetector devices directly from our mechanosynthesized perovskites and evaluated their performances by conducting photocurrent measurements. The devices can be readily made by mechanically compressing the perovskite powders into small disks using a hydraulic pelleting press under an inert N_2 atmosphere. Subsequently, gold electrodes were then vapor deposited onto the disks to create an active device area of 8.0×10^{-3} cm^2 (Figures 7A and S18). The photocurrent measurements of the devices were then conducted under the illumination of a 445-nm light-emitting diode lamp *in vacuo*. Among the examined tin-based devices, $CsSnBr_{1.5}Cl_{1.5}$ performed the best (Figure 7B) and exhibited nearly 10 times as much current (44.3 nA) under illumination than in the dark (4.94 nA). The device also displayed on-off responsiveness without significant hysteresis during the working cycles (Figure 7B), with an overall responsivity and detectivity of 8.1×10^{-2} $mA\cdot W^{-1}$ and 1.8×10^{-8} Jones, respectively.

Nevertheless, owing to the limitations of the instrumental setups, short-term exposure of these devices to air for several seconds was inevitable, which could cause Sn(II) oxidation on the exposed top surfaces. The small amounts of Sn(IV), which could be detected by XPS experiments, were likely to be the cause of the high dark current that we detected. However, we highlight that these tin-based perovskites' device

performance data have not been determined or reported previously. Moreover, the solution-processed thin-film devices made by spin-coating could not be evaluated conclusively owing to the poor solubility of the perovskite powders and their precursor salts. The solution-based processing methods are known to be affected by problems such as reproducibility, oxidation, and phase impurities of the thin films (Figure S19), especially for tin-based perovskites (Sabba et al., 2015), which will impede their widespread applicability in optoelectronic devices. Through simple utilization of a hydraulic press, we were able to demonstrate a proof of concept for an entirely solvent-free prototype fabrication from commercially available precursor salts of the perovskites.

Although the state-of-the-art for perovskite photodetectors remain as Pb-based devices, the necessity for toxic Pb is patently undesirable. Some recent examples of Pb-free photodetectors were reported, but they contain hydrolytically and thermally unstable organic ammonium cations (Fang et al., 2019; Ji et al., 2018; Waleed et al., 2017; Wang et al., 2019; Yang et al., 2018). Thus we have illustrated the first green, Pb-free, all-inorganic perovskite functional photodetector, and only the second instance of an entirely solvent-free perovskite device fabrication (Chen et al., 2017). This employment of mechanochemical ball milling combined with the use of a hydraulic press represents a pioneering synthetic protocol to fabricate a functional device from metal salt precursors in a completely solvent-free and feasibly scalable manner.

Conclusions

In summary, we have developed a mechanochemical protocol for the rapid, solvent-free, general synthesis of multiple metal halide perovskites, which can be produced at up to kilogram scales. Critically, even metastable perovskites were achieved mechanochemically in high purity under ambient conditions while circumventing the need for additives or post-synthetic thermal treatment. Moreover, we fabricated a photodetector device from these powders via a hydraulic press, creating the first functional device based on an all-inorganic, Pb-free perovskite, establishing a completely solvent-free protocol starting from commercially available precursor salts. These results highlight the prominent advantages of our mechanochemical approach for the synthesis of perovskites and underscore the promise of mechanochemistry for the large-scale fabrication of perovskite devices. We believe that our solvent-free mechanochemical methodology can dramatically reduce the energetic and environmental footprint for the fabrication of perovskite devices and pave the way for broader adoption by industry in the future.

Limitations of the Study

Although we demonstrated that mechanochemical synthesis can be applied to prepare air-, moisture-, and thermally sensitive metal halide perovskites, these materials require stringent handling under an inert atmosphere. Many of the materials that we examined, especially the metastable ones, cannot be readily incorporated into devices without additional encapsulation and other fabrication procedures, which could increase the environmental footprint. Nonetheless, this study illustrates a proof-of-concept about the versatility of mechanochemical synthesis, not only for stable materials but also for ostensibly sensitive compounds.

METHODS

All methods can be found in the accompanying Transparent Methods supplemental file.

SUPPLEMENTAL INFORMATION

Supplemental Information can be found online at https://doi.org/10.1016/j.isci.2019.05.042.

ACKNOWLEDGMENTS

H.S.S. is supported by MOE Tier 1 grants RG 13/17 and RG 111/18. H.S.S. also acknowledges the Agency for Science, Technology and Research (A*STAR) and AME IRG grants A1783c0002 and A1783c0007 for funding this research. The authors are grateful for support from the Solar Fuels Lab at NTU. F.G. acknowledges an A*STAR AME IRG A1783c0003 and an NTU start-up grant M4080552 for financial support. N.M. and R.A.J. acknowledge the funding from MOE Tier 1 grant RG 166/16, MOE Tier 2 grants MOE2016-T2-1-100 and MOE2015-T2-2-007, and the National Research Foundation under NRF RF Award No. NRF-RF2013-08. T.C.S. and Y.K.E.T. acknowledge funding support from an MOE Tier 1 grant RG 173/16 and MOE Tier 2 grants MOE2015-T2-2-015 and MOE2016-T2-1-034. We also thank Mr. Leonard Kia-Sheun Ng for help with the SEM-EDX experiments. We thank Prof. Yeng Ming Lam and Dr. Bing Bing Chen for help with electrode deposition.

AUTHOR CONTRIBUTIONS

H.S.S., F.G., and N.M. conceived the research. H.S.S. and F.G. obtained the funding for the project and jointly supervised Z.H. and D.T. Z.H. and D.T. designed the experiments. Z.H., D.T., and Y.K.T.H. performed the synthetic and characterization experiments and conducted the photophysical measurements. R.A.J. collected the photoelectrical data and analyzed the results. Y.K.E.T collected the PL and TRPL data and analyzed the results. All authors analyzed the data and participated in drafting and revising the manuscript.

DECLARATION OF INTERESTS

The authors declare no competing interests.

Received: November 7, 2018
Revised: May 22, 2019
Accepted: May 30, 2019
Published: June 28, 2019

REFERENCES

Askar, A.M., Karmakar, A., Bernard, G.M., Ha, M., Terskikh, V.V., Wiltshire, B.D., Patel, S., Fleet, J., Shankar, K., and Michaelis, V.K. (2018). Composition-Tunable formamidinium lead mixed halide perovskites via solvent-free mechanochemical synthesis: decoding the Pb environments using solid-state NMR spectroscopy. J. Phys. Chem. Lett. *9*, 2671–2677.

Avvakumov, G.V., Senna, M., and Kosova, N.V. (2001). Soft Mechanochemical Synthesis: A Basis for New Chemical Technologies (Springer Science & Business Media).

Baláž, P. (2008). Mechanochemistry and nanoscience. In Mechanochemistry in Nanoscience and Minerals Engineering (Springer), pp. 1–102.

Balaz, P., Achimovicova, M., Balaz, M., Billik, P., Cherkezova-Zheleva, Z., Criado, J.M., Delogu, F., Dutkova, E., Gaffet, E., Gotor, F.J., et al. (2013). Hallmarks of mechanochemistry: from nanoparticles to technology. Chem. Soc. Rev. *42*, 7571–7637.

Bi, C., Wang, Q., Shao, Y., Yuan, Y., Xiao, Z., and Huang, J. (2015). Non-wetting surface-driven high-aspect-ratio crystalline grain growth for efficient hybrid perovskite solar cells. Nat. Commun. *6*, 7747.

Boldyrev, V.V. (2006). Mechanochemistry and mechanical activation of solids. Russ. Chem. Rev. *75*, 177–189.

Boldyrev, V.V., and Tkáčová, K. (2000). Mechanochemistry of solids: past, present, and prospects. J. Mater. Synth. Process. *8*, 121–132.

Boldyreva, E. (2013). Mechanochemistry of inorganic and organic systems: what is similar, what is different? Chem. Soc. Rev. *42*, 7719–7738.

Chen, H., Ye, F., Tang, W., He, J., Yin, M., Wang, Y., Xie, F., Bi, E., Yang, X., Gratzel, M., et al. (2017). A solvent- and vacuum-free route to large-area perovskite films for efficient solar modules. Nature *550*, 92–95.

Correa-Baena, J.P., Saliba, M., Buonassisi, T., Gratzel, M., Abate, A., Tress, W., and Hagfeldt, A. (2017). Promises and challenges of perovskite solar cells. Science *358*, 739–744.

Crawford, D., Casaban, J., Haydon, R., Giri, N., McNally, T., and James, S.L. (2015). Synthesis by extrusion: continuous, large-scale preparation of MOFs using little or no solvent. Chem. Sci. *6*, 1645–1649.

Deng, H., Yang, X.K., Dong, D.D., Li, B., Yang, D., Yuan, S.J., Qiao, K.K., Cheng, Y.B., Tang, J., and Song, H.S. (2015). Flexible and semitransparent organolead triiodide perovskite network photodetector arrays with high stability. Nano Lett. *15*, 7963–7969.

Do, J.L., and Friscic, T. (2017). Mechanochemistry: a force of synthesis. ACS Cent. Sci. *3*, 13–19.

Dohner, E.R., Jaffe, A., Bradshaw, L.R., and Karunadasa, H.I. (2014). Intrinsic white-light emission from layered hybrid perovskites. J. Am. Chem. Soc. *136*, 13154–13157.

Dokic, M., and Soo, H.S. (2018). Artificial photosynthesis by light absorption, charge separation, and multielectron catalysis. Chem. Commun. (Camb.) *54*, 6554–6572.

Dualeh, A., Gao, P., Seok, S.I., Nazeeruddin, M.K., and Grätzel, M. (2014). Thermal behavior of methylammonium lead-trihalide perovskite photovoltaic light harvesters. Chem. Mater. *26*, 6160–6164.

El Ajjouri, Y., Chirvony, V.S., Sessolo, M., Palazon, F., and Bolink, H.J. (2018a). Incorporation of potassium halides in the mechanosynthesis of inorganic perovskites: feasibility and limitations of ion-replacement and trap passivation. RSC Adv. *8*, 41548–41551.

El Ajjouri, Y., Palazon, F., Sessolo, M., and Bolink, H.J. (2018b). Single-source vacuum deposition of mechanosynthesized inorganic halide perovskites. Chem. Mater. *30*, 7423–7427.

Fang, C., Wang, H., Shen, Z., Shen, H., Wang, S., Ma, J., Wang, J., Luo, H., and Li, D. (2019). High-performance photodetectors based on lead-free 2D ruddlesden-popper perovskite/MoS2 heterostructures. ACS Appl. Mater. Interfaces *11*, 8419–8427.

Friscic, T., Trask, A.V., Jones, W., and Motherwell, W.D. (2006). Screening for inclusion compounds and systematic construction of three-component solids by liquid-assisted grinding. Angew. Chem. Int. Ed. *45*, 7546–7550.

Gazi, S., Dokic, M., Moeljadi, A.M.P., Ganguly, R., Hirao, H., and Soo, H.S. (2017). Kinetics and DFT studies of photoredox carbon-carbon bond cleavage reactions by molecular vanadium catalysts under ambient conditions. ACS Catal. *7*, 4682–4691.

Geciauskaite, A.A., and Garcia, F. (2017). Main group mechanochemistry. Beilstein J. Org. Chem. *13*, 2068–2077.

Granger, P., Parvulescu, V.I., Parvulescu, V.I., and Prellier, W. (2016). Perovskites and Related Mixed Oxides: Concepts and Applications. https://www.wiley.com/en-sg/Perovskites+and+Related+Mixed+Oxides:+Concepts+and+Applications-p-9783527337637.

Han, Q., Bae, S.H., Sun, P., Hsieh, Y.T., Yang, Y.M., Rim, Y.S., Zhao, H., Chen, Q., Shi, W., Li, G., et al. (2016). Single crystal formamidinium lead iodide ($FAPbI_3$): insight into the structural, optical, and electrical properties. Adv. Mater. *28*, 2253–2258.

Heinicke, V.G. (1984). Tribochemistry: Translation from German (Akademie-Verlag).

Hernandez, J.G., and Bolm, C. (2017). Altering product selectivity by mechanochemistry. J. Org. Chem. *82*, 4007–4019.

Hong, Z., Chong, W.K., Ng, A.Y.R., Li, M., Ganguly, R., Sum, T.C., and Soo, H.S. (2019). Hydrophobic metal halide perovskites for visible-light photoredox C-C bond cleavage and dehydrogenation catalysis. Angew. Chem. Int. Ed. *58*, 3456–3460.

James, S.L., Adams, C.J., Bolm, C., Braga, D., Collier, P., Friscic, T., Grepioni, F., Harris, K.D., Hyett, G., Jones, W., et al. (2012). Mechanochemistry: opportunities for new and cleaner synthesis. Chem. Soc. Rev. *41*, 413–447.

Jana, A., Mittal, M., Singla, A., and Sapra, S. (2017). Solvent-free, mechanochemical syntheses of bulk trihalide perovskites and their nanoparticles. Chem. Commun. (Camb.) *53*, 3046–3049.

Ji, C., Wang, P., Wu, Z., Sun, Z., Li, L., Zhang, J., Hu, W., Hong, M., and Luo, J. (2018). Inch-size single crystal of a lead-free organic–inorganic hybrid perovskite for high-performance photodetector. Adv. Funct. Mater. *28*, 1705467.

Jodlowski, A.D., Yepez, A., Luque, R., Camacho, L., and de Miguel, G. (2016). Benign-by-design solventless mechanochemical synthesis of three-, two-, and one-dimensional hybrid perovskites. Angew. Chem. Int. Ed. *55*, 14972–14977.

Jones, W., and Eddleston, M.D. (2014). Introductory lecture: mechanochemistry, a versatile synthesis strategy for new materials. Faraday Discuss. *170*, 9–34.

Karmakar, A., Askar, A.M., Bernard, G.M., Terskikh, V.V., Ha, M., Patel, S., Shankar, K., and Michaelis, V.K. (2018). Mechanochemical synthesis of methylammonium lead mixed–halide perovskites: unraveling the solid-solution behavior using solid-state NMR. Chem. Mater. *30*, 2309–2321.

Karmakar, A., Dodd, M.S., Zhang, X., Oakley, M.S., Klobukowski, M., and Michaelis, V.K. (2019). Mechanochemical synthesis of 0D and 3D cesium lead mixed halide perovskites. Chem. Commun. (Camb.) *55*, 5079–5082.

Koh, T.M., Thirumal, K., Soo, H.S., and Mathews, N. (2016). Multidimensional perovskites: a mixed cation approach towards ambient stable and tunable perovskite photovoltaics. ChemSusChem *9*, 2541–2558.

Kojima, A., Teshima, K., Shirai, Y., and Miyasaka, T. (2009). Organometal halide perovskites as visible-light sensitizers for photovoltaic cells. J. Am. Chem. Soc. *131*, 6050–6051.

Konstantakou, M., and Stergiopoulos, T. (2017). A critical review on tin halide perovskite solar cells. J. Mater. Chem. A *5*, 11518–11549.

Leguy, A.M.A., Hu, Y., Campoy-Quiles, M., Alonso, M.I., Weber, O.J., Azarhoosh, P., van Schilfgaarde, M., Weller, M.T., Bein, T., Nelson, J., et al. (2015). Reversible hydration of $CH_3NH_3PbI_3$ in films, single crystals, and solar cells. Chem. Mater. *27*, 3397–3407.

Leong, W.L., Ooi, Z.E., Sabba, D., Yi, C., Zakeeruddin, S.M., Graetzel, M., Gordon, J.M., Katz, E.A., and Mathews, N. (2016). Identifying fundamental limitations in halide perovskite solar cells. Adv. Mater. *28*, 2439–2445.

Lim, J.H., Engelmann, X., Corby, S., Ganguly, R., Ray, K., and Soo, H.S. (2018). C-H activation and nucleophilic substitution in a photochemically generated high valent iron complex. Chem. Sci. *9*, 3992–4002.

Liu, J.Y., Xue, Y.Z., Wang, Z.Y., Xu, Z.Q., Zheng, C.X., Weber, B., Song, J.C., Wang, Y.S., Lu, Y.R., Zhang, Y.P., et al. (2016). Two-dimensional $CH_3NH_3PbI_3$ perovskite: synthesis and optoelectronic application. ACS Nano *10*, 3536–3542.

Manukyan, K.V., Yeghishyan, A.V., Moskovskikh, D.O., Kapaldo, J., Mintairov, A., and Mukasyan, A.S. (2016). Mechanochemical synthesis of methylammonium lead iodide perovskite. J. Mater. Sci. *51*, 9123–9130.

McMeekin, D.P., Sadoughi, G., Rehman, W., Eperon, G.E., Saliba, M., Horantner, M.T., Haghighirad, A., Sakai, N., Korte, L., Rech, B., et al. (2016). A mixed-cation lead mixed-halide perovskite absorber for tandem solar cells. Science *351*, 151–155.

Muñoz-Batista, M.J., Rodriguez-Padron, D., Puente-Santiago, A.R., and Luque, R. (2018). Mechanochemistry: toward sustainable design of advanced nanomaterials for electrochemical energy storage and catalytic applications. ACS Sustain. Chem. Eng. *6*, 9530–9544.

Ng, Y.Y., Tan, L.J., Ng, S.M., Chai, Y.T., Ganguly, R., Du, Y., Yeow, E.K.L., and Soo, H.S. (2018). Spectroscopic characterization and mechanistic studies on visible light photoredox carbon–carbon bond formation by Bis(arylimino) acenaphthene copper photosensitizers. ACS Catal. *8*, 11277–11286.

Noel, N.K., Abate, A., Stranks, S.D., Parrott, E.S., Burlakov, V.M., Goriely, A., and Snaith, H.J. (2014). Enhanced photoluminescence and solar cell performance via lewis base passivation of organic–inorganic lead halide perovskites. ACS Nano *8*, 9815–9821.

Pal, P., Saha, S., Banik, A., Sarkar, A., and Biswas, K. (2018). All-solid-state mechanochemical synthesis and post-synthetic transformation of inorganic perovskite-type halides. Chem. Eur. J. *24*, 1811–1815.

Peedikakkandy, L., and Bhargava, P. (2016). Composition dependent optical, structural and photoluminescence characteristics of cesium tin halide perovskites. RSC Adv. *6*, 19857–19860.

Posudievsky, O.Y., Konoshchuk, N.V., Karbivskyy, V.L., Boiko, O.P., Koshechko, V.G., and Pokhodenko, V.D. (2017). Structural and spectral characteristics of mechanochemically prepared CsPbBr3. Theor. Exp. Chem. *53*, 235–243.

Pradhan, N., Dutta, A., Dutta, S.K., and Das Adhikari, S. (2018). Phase Stable $CsPbI_3$ nanocrystals: the reaction temperature matters. Angew. Chem. Int. Ed. *57*, 1–6.

Prochowicz, D., Franckevičius, M., Cieślak, A.M., Zakeeruddin, S.M., Grätzel, M., and Lewiński, J. (2015). Mechanosynthesis of the hybrid perovskite $CH_3NH_3PbI_3$: characterization and the corresponding solar cell efficiency. J. Mater. Chem. A *3*, 20772–20777.

Prochowicz, D., Yadav, P., Saliba, M., Kubicki, D.J., Tavakoli, M.M., Zakeeruddin, S.M., Lewiński, J., Emsley, L., and Grätzel, M. (2018). One-step mechanochemical incorporation of an insoluble cesium additive for high performance planar heterojunction solar cells. Nano Energy *49*, 523–528.

Prochowicz, D., Yadav, P., Saliba, M., Saski, M., Zakeeruddin, S.M., Lewiński, J., and Grätzel, M. (2017). Mechanosynthesis of pure phase mixed-cation MAxFA1−xPbI3 hybrid perovskites: photovoltaic performance and electrochemical properties. Sustain. Energy Fuels *1*, 689–693.

Protesescu, L., Yakunin, S., Nazarenko, O., Dirin, D.N., and Kovalenko, M.V. (2018). Low-cost synthesis of highly luminescent colloidal lead halide perovskite nanocrystals by wet ball milling. ACS Appl. Nano Mater. *1*, 1300–1308.

Rosales, B.A., Wei, L., and Vela, J. (2019). Synthesis and mixing of complex halide perovskites by solvent-free solid-state methods. J. Solid State Chem. *271*, 206–215.

Sabba, D., Mulmudi, H.K., Prabhakar, R.R., Krishnamoorthy, T., Baikie, T., Boix, P.P., Mhaisalkar, S., and Mathews, N. (2015). Impact of anionic Br^- substitution on open circuit voltage in lead free perovskite ($CsSnI_3$-xBr_x) solar cells. J. Phys. Chem. C *119*, 1763–1767.

Sadhukhan, P., Kundu, S., Roy, A., Ray, A., Maji, P., Dutta, H., Pradhan, S.K., and Das, S. (2018). Solvent-free solid-state synthesis of high yield mixed halide perovskites for easily tunable composition and band gap. Cryst. Growth Des. *18*, 3428–3432.

Scaife, D.E., Weller, P.F., and Fisher, W.G. (1974). Crystal preparation and properties of cesium tin(II) trihalides. J. Solid State Chem. *9*, 308–314.

Senna, M. (1993). Incipient chemical interaction between fine particles under mechanical stress - a feasibility of producing advanced materials via mechanochemical routes. Solid State Ion. *63-65*, 3–9.

Shi, Y.X., Xu, K., Clegg, J.K., Ganguly, R., Hirao, H., Friscic, T., and Garcia, F. (2016). The first synthesis of the sterically encumbered adamantoid phosphazane $P_4(N^tBu)_6$: enabled by mechanochemistry. Angew. Chem. Int. Ed. *55*, 12736–12740.

Sim, Y., Shi, Y.X., Ganguly, R., Li, Y., and García, F. (2017). Mechanochemical synthesis of phosphazane-based frameworks. Chem. Eur. J. *23*, 11279–11285.

Sim, Y., Tan, D., Ganguly, R., Li, Y., and García, F. (2018). Orthogonality in main group compounds: a direct one-step synthesis of air- and moisture-stable cyclophosphazanes by mechanochemistry. Chem. Commun. (Camb.) *54*, 6800–6803.

Stoumpos, C.C., Malliakas, C.D., and Kanatzidis, M.G. (2013). Semiconducting tin and lead iodide perovskites with organic cations: phase transitions, high mobilities, and near-infrared photoluminescent properties. Inorg. Chem. *52*, 9019–9038.

Su, L., Zhao, Z.X., Li, H.Y., Yuan, J., Wang, Z.L., Cao, G.Z., and Zhu, G. (2015). High-performance organolead halide perovskite-based self-powered triboelectric photodetector. ACS Nano *9*, 11310–11316.

Takacs, L. (2002). Self-sustaining reactions induced by ball milling. Prog. Mater. Sci. *47*, 355–414.

Tan, D., and Garcia, F. (2019). Main group mechanochemistry: from curiosity to established protocols. Chem. Soc. Rev. *48*, 2274–2292.

Tan, Z.K., Moghaddam, R.S., Lai, M.L., Docampo, P., Higler, R., Deschler, F., Price, M., Sadhanala, A., Pazos, L.M., Credgington, D., et al. (2014). Bright light-emitting diodes based on organometal halide perovskite. Nat. Nanotechnol. *9*, 687–692.

Tanaka, A. (2004). Toxicity of indium arsenide, gallium arsenide, and aluminium gallium arsenide. Toxicol. Appl. Pharmacol. *198*, 405–411.

Thirumal, K., Chong, W.K., Xie, W., Ganguly, R., Muduli, S.K., Sherburne, M., Asta, M., Mhaisalkar, S., Sum, T.C., Soo, H.S., et al. (2017). Morphology-independent stable white-light emission from self-assembled two-dimensional perovskites driven by strong exciton–phonon coupling to the organic framework. Chem. Mater. *29*, 3947–3953.

Tkáčová, K. (1989). Mechanical Activation of Minerals (Developments in Mineral Processing) (Elsevier Science Ltd.).

Waleed, A., Tavakoli, M.M., Gu, L., Wang, Z., Zhang, D., Manikandan, A., Zhang, Q., Zhang, R., Chueh, Y.L., and Fan, Z. (2017). Lead-Free perovskite nanowire array photodetectors with drastically improved stability in nanoengineering templates. Nano Lett. *17*, 523–530.

Wang, J.Y., Ganguly, R., Li, Y.X., Diaz, J., Soo, H.S., and Garcia, F. (2016). A multi-step solvent-free mechanochemical route to indium(III) complexes. Dalton Trans. *45*, 7941–7946.

Wang, J.Y., Ganguly, R., Li, Y.X., Diaz, J., Soo, H.S., and Garcia, F. (2017). Synthesis and the optical and electrochemical properties of indium(III) Bis(arylimino)acenaphthene complexes. Inorg. Chem. *56*, 7811–7820.

Wang, Y., Yang, D., Ma, D., Kim, D.H., Ahamad, T., Alshehri, S.M., and Vadim, A. (2019). Organic-inorganic hybrid Sn-based perovskite photodetectors with high external quantum efficiencies and wide spectral responses from 300 to 1000 nm. Sci. China Mater. *62*, 790–796.

Wang, Y.S., Zhang, Y.P., Lu, Y., Xu, W.D., Mu, H.R., Chen, C.Y., Qiao, H., Song, J.C., Li, S.J., Sun, B.Q., et al. (2015). Hybrid graphene-perovskite phototransistors with ultrahigh responsivity and gain. Adv. Opt. Mater. *3*, 1389–1396.

Weber, O.J., Ghosh, D., Gaines, S., Henry, P.F., Walker, A.B., Islam, M.S., and Weller, M.T. (2018). Phase behavior and polymorphism of formamidinium lead iodide. Chem. Mater. *30*, 3768–3778.

Xing, G., Mathews, N., Lim, S.S., Yantara, N., Liu, X., Sabba, D., Grätzel, M., Mhaisalkar, S., and Sum, T.C. (2014). Low-temperature solution-processed wavelength-tunable perovskites for lasing. Nat. Mater. *13*, 476–480.

Yang, B., Li, Y.J., Tang, Y.X., Mao, X., Luo, C., Wang, M.S., Deng, W.Q., and Han, K.L. (2018). Constructing sensitive and fast lead-free single-crystalline perovskite photodetectors. J. Phys. Chem. Lett. *9*, 3087–3092.

Yang, J.L., Siempelkamp, B.D., Liu, D.Y., and Kelly, T.L. (2015a). Investigation of $CH_3NH_3PbI_3$ degradation rates and mechanisms in controlled humidity environments using in situ techniques. ACS Nano *9*, 1955–1963.

Yang, W.S., Noh, J.H., Jeon, N.J., Kim, Y.C., Ryu, S., Seo, J., and Seok, S.I. (2015b). SOLAR CELLS. High-performance photovoltaic perovskite layers fabricated through intramolecular exchange. Science *348*, 1234–1237.

Yang, W.S., Park, B.W., Jung, E.H., Jeon, N.J., Kim, Y.C., Lee, D.U., Shin, S.S., Seo, J., Kim, E.K., Noh, J.H., et al. (2017). Iodide management in formamidinium-lead-halide-based perovskite layers for efficient solar cells. Science *356*, 1376–1379.

Yantara, N., Bhaumik, S., Yan, F., Sabba, D., Dewi, H.A., Mathews, N., Boix, P.P., Demir, H.V., and Mhaisalkar, S. (2015). Inorganic halide perovskites for efficient light-emitting diodes. J. Phys. Chem. Lett. *6*, 4360–4364.

Yun, S., Kirakosyan, A., Yoon, S.-G., and Choi, J. (2018). Scalable synthesis of exfoliated organometal halide perovskite nanocrystals by ligand-assisted ball milling. ACS Sustain. Chem. Eng. *6*, 3733–3738.

Zhang, R., Fan, J.D., Zhang, X., Yu, H.H., Zhang, H.J., Mai, Y.H., Xu, T.X., Wang, J.Y., and Snaith, H.J. (2016). Nonlinear optical response of organic-inorganic halide perovskites. ACS Photonics *3*, 371–377.

Zhou, H., Chen, Q., Li, G., Luo, S., Song, T.B., Duan, H.S., Hong, Z., You, J., Liu, Y., and Yang, Y. (2014). Photovoltaics. Interface engineering of highly efficient perovskite solar cells. Science *345*, 542–546.

Zhu, H.M., Fu, Y.P., Meng, F., Wu, X.X., Gong, Z.Z., Ding, Q., Gustafsson, M.V., Trinh, M.T., Jin, S., and Zhu, X.Y. (2015). Lead halide perovskite nanowire lasers with low lasing thresholds and high quality factors. Nat. Mater. *14*, 636–642.

Zhu, Z.Y., Yang, Q.Q., Gao, L.F., Zhang, L., Shi, A.Y., Sun, C.L., Wang, Q., and Zhang, H.L. (2017). Solvent-free mechanosynthesis of composition-tunable cesium lead halide perovskite quantum dots. J. Phys. Chem. Lett. *8*, 1610–1614.

ISCI, Volume *16*

Supplemental Information

Completely Solvent-free Protocols to Access Phase-Pure, Metastable Metal Halide Perovskites and Functional Photodetectors from the Precursor Salts

Zonghan Hong, Davin Tan, Rohit Abraham John, Yong Kang Eugene Tay, Yan King Terence Ho, Xin Zhao, Tze Chien Sum, Nripan Mathews, Felipe García, and Han Sen Soo

Supplemental Information

Supplemental data

Table S1. Detailed evaluation of the state-of-the-art in mechanochemical synthesis of metal halide perovskites. Related to Table 1.

Citation in manuscript	Perovskites prepared	Stability or post-synthetic processing methods	Focus of study	Application
(Karmakar et al., 2018)	$MAPbBr_xCl_{3-x}$	All thermally stable phases	Solid-state ^{207}Pb NMR spectroscopy correlated to crystal structures	None
(Pal et al., 2018)	3D $CsPbBr_3$, 2D $CsPb2Br_5$, 0D Cs_4PbBr_6, 3D $CsPbCl_3$, 2D $CsPb_2Cl_5$, 0D Cs_4PbCl_6, 3D $CsPbI_3$, and 3D $RbPbI_3$	All thermally stable phases	Pb-based perovskites of all dimensions from 3D to 0D prepared; interconversion between dimensions by mechanochemistry	None
(Jana et al., 2017)	$APbBr_3$ (A = Cs, MA, FA)	All thermally stable phases, octylammonium surfactants used to stabilize nanoparticles	Different bulk microcrystalline morphologies; access to nanoparticles	None
(Askar et al., 2018)	$FAPbX_3$ (X = Cl, Br, I) and their mixed halides	Mostly thermally stable phases; some metastable examples accessed by post-synthetic annealing	Solid-state ^{207}Pb NMR spectroscopy correlated to crystal structures	None
(El Ajjouri et al., 2018a)	$Cs_{1-x}K_xPbBr_{3-y}X_y$ (X = I, Br, Cl)	All thermally stable phases	Use of K cations to passivate traps	None
38(El Ajjouri et al., 2018b)	$CsPbX_3$ (X = Cl, Br, I)	All thermally stable except $CsPbI_3$; vaporization and thermal annealing to access thin films	Use of single sources for vacuum deposition of mechanochemically prepared perovskites	None
(Prochowicz et al., 2018)	$CsPbCl_3$, $CsPbBr_3$, $CsPbBr_{1.5}Cl_{1.5}$, and mixed ion $FA_xMA_{1-x}CsPbI_yBr_{3-y}$	All thermally stable phases; post-synthetic solution processing in DMSO/DMF to prepare solar cells	High efficiency solar cells with Cs additives derived from mechanochemically prepared powders	Solar cell
(Prochowicz et al., 2017)	$MA_xFA_{1-x}PbI_3$	Mostly stable phases; MA added to stabilize α-$FAPbI_3$; solution processing to prepare solar cells	Development of solar cells with perovskites derived from mechanochemistry	Solar cell
(Protesescu et al., 2018)	$FAPbBr_3$ and $CsPbBr_3$	All thermally stable phases, octylammonium surfactants used to stabilize nanoparticles	Mechanochemical synthesis of highly luminescent nanocrystals	None
(Sadhukhan et al., 2018)	$MAPbI_xBr_{3-x}$	All thermally stable phases	Band gap tuning by changing relative halide composition	None
(Yun et al., 2018)	$MAPbBr_3$ and $FAPbBr_3$	All thermally stable phases, octylammonium and octadecylammonium surfactants used to stabilize nanoparticles	Surfactant assisted exfoliation to access luminescent nanocrystals	None
(Posudievsky et al., 2017)	$CsPbBr_3$	Stable nanoparticles, processed in DMF	Nanoparticles prepared by mechanochemistry	None

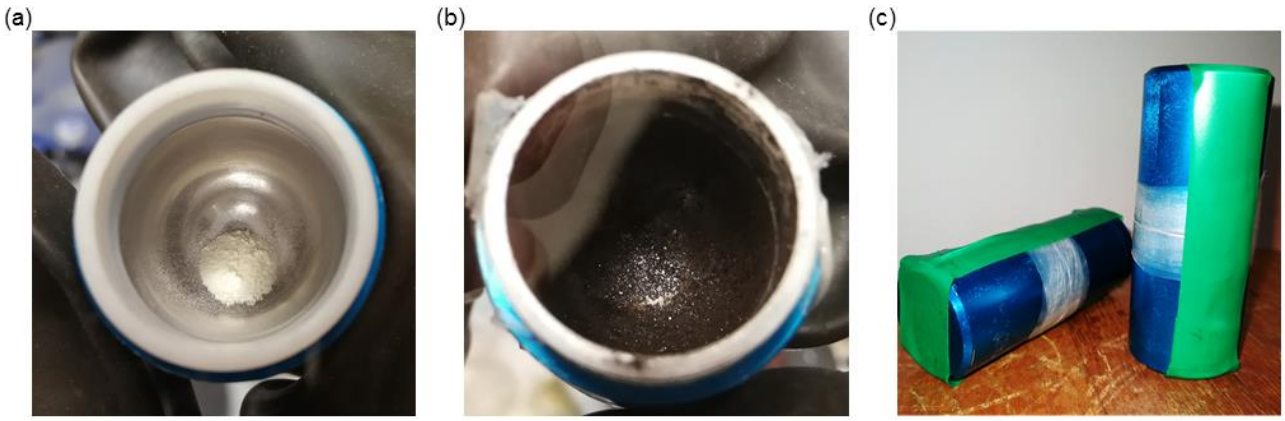

Figure S1. Photographs of the mechanochemical synthesis of $CsSnBr_3$ as an example (a) before and (b) after ball milling; (c) milling jars were sealed with paraffin film and electrical tape to prevent exposure to air. Related to Figure 1.

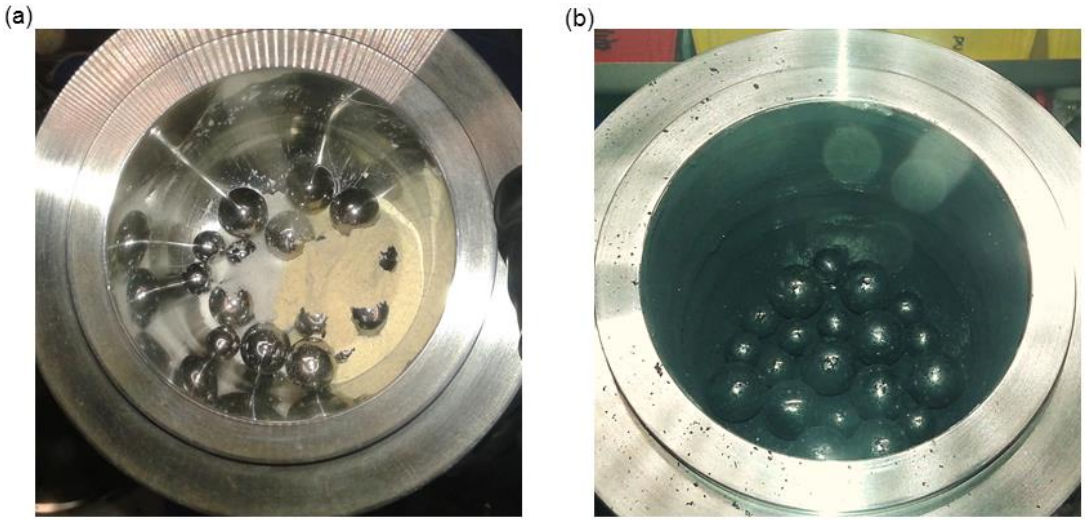

Figure S2. Photographs of the large-scale (25 g) synthesis of $CsSnBr_3$ (a) before and (b) after ball milling. Related to Figures 1 and 4.

Figure S3. Photographic demonstration of the kg-scale synthesis of $CsSnBr_{1.5}Cl_{1.5}$. a) Preparation of the reagents CsBr, CsCl, $SnBr_2$, and $SnCl_2$ (all white powders) in a N_2 glovebox. The reagents were weighed and transferred from a beaker into the 250 mL mechanochemical reaction vessel. The total reagent weight was 250 g. b) The reagent mixture with the milling balls at the bottom of the vessel. c) Gentle mixing of the reagents, which exposed the milling balls, by using a metal spatula. d) Planetary mill containing four reaction vessel holders, essentially allowing four 250 g reactions to take place simultaneously, leading to a 1.0 kg scale batch synthesis of the perovskite. e) The orange product after 10 hr of milling. Related to Figures 1 and 4.

PXRD studies of control experiments

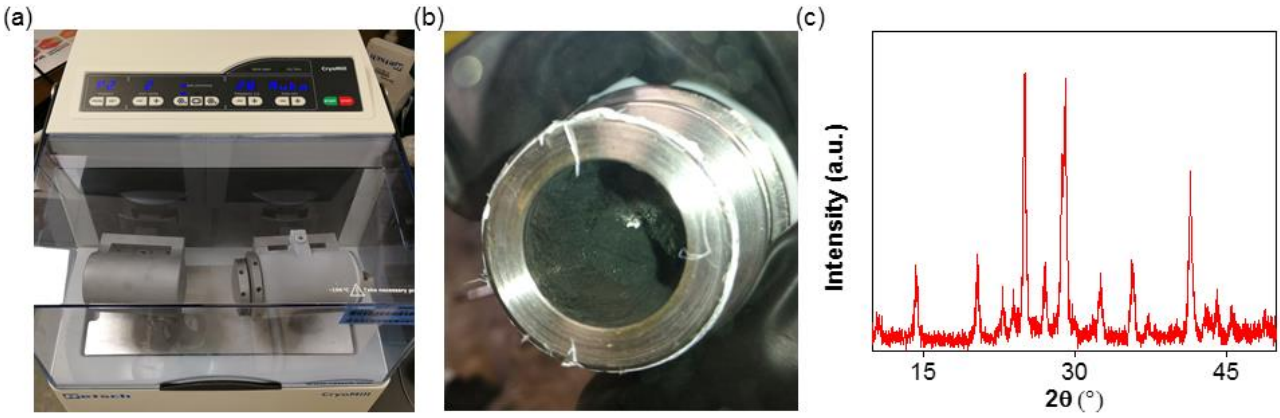

Figure S4. Photographs and data of the cryomilling synthesis of $CsSnI_3$. (a) Photograph of cryomilling setup with liquid N_2 flow. (b) Photograph showing the black perovskite phase product obtained by cryomilling. (c) PXRD pattern of the product from cryomilling, showing a pure orthorhombic (black) phase. Related to Figure 2.

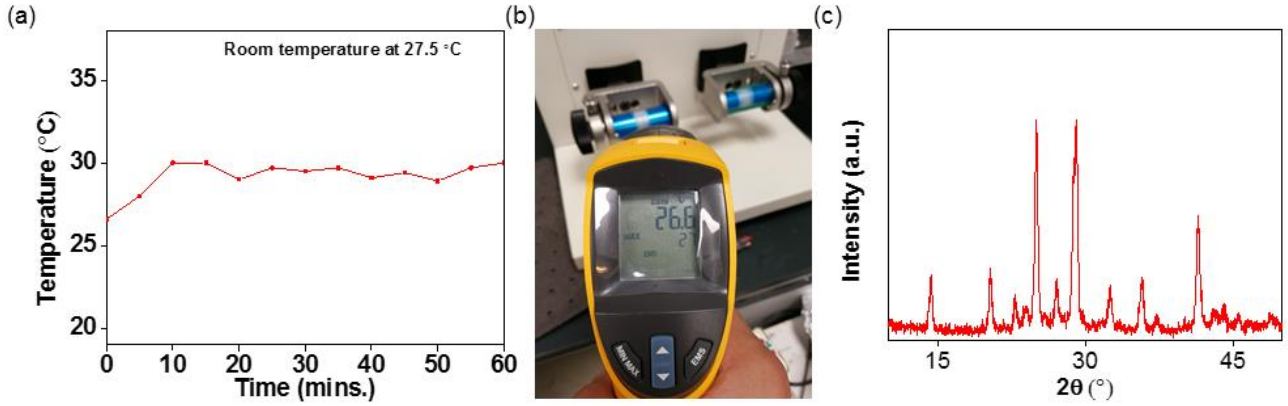

Figure S5. Controlled-temperature mechanochemical synthesis of $CsSnI_3$. (a) Reaction temperature monitored over 1 hr during a milling experiment. The milling jars were then allowed to cool down to below 28 °C every 5 min before the milling resumed. (b) Photograph of a reaction monitored by an IR thermometer. (c) PXRD pattern of the product showing a pure orthorhombic (black) phase. Related to Figure 2.

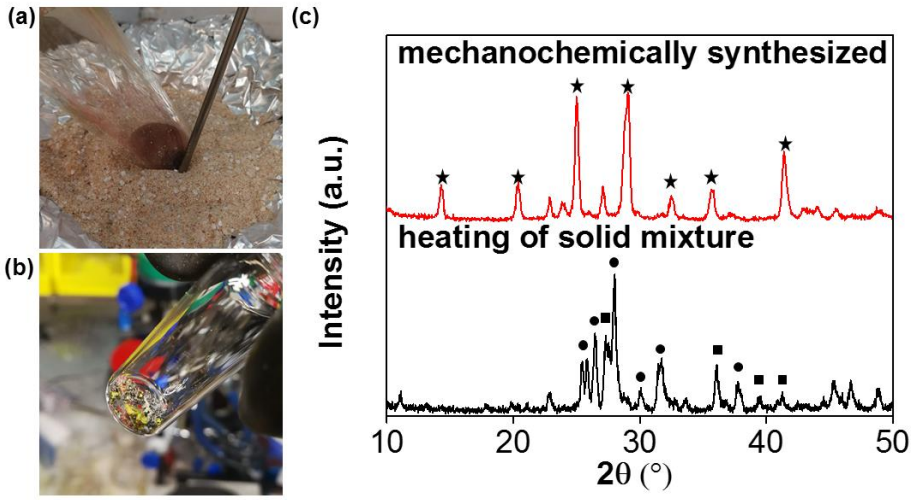

Figure S6. Control experiments for the attempted synthesis of $CsSnI_3$ perovskite with heat only under solvent-free conditions. (a) Photograph of the solid reaction mixture being heated in a sand-bath equipped with a temperature sensor. (b) Photograph of the resulting product after heating to 320 ºC for 1 h, showing a multi–colored solid. (c) Comparison of the PXRD patterns of the perovskite powder that was synthesized mechanochemically (red line) and the heated solid product (black line). Multiple compounds can be identified from the thermal reaction, including SnI_2 and $CsSnI_3$ in the yellow orthorhombic phase as the major components. Related to Figure 2.

XPS experiments and data

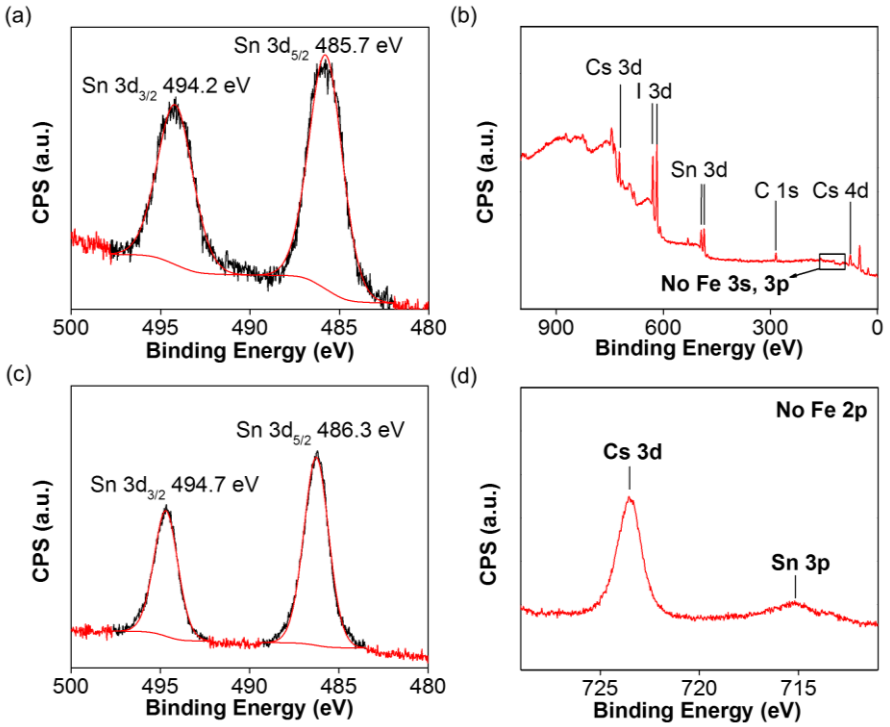

Figure S7. (a) Sn 3d XPS data for $CsSnI_3$. (b) Survey spectrum of $CsSnI_3$. (c) Sn 3d XPS data in $CsSnI_3$ after being exposed to air. (d) no Fe was detected in the 2p range. Related to Figures 2 and 3.

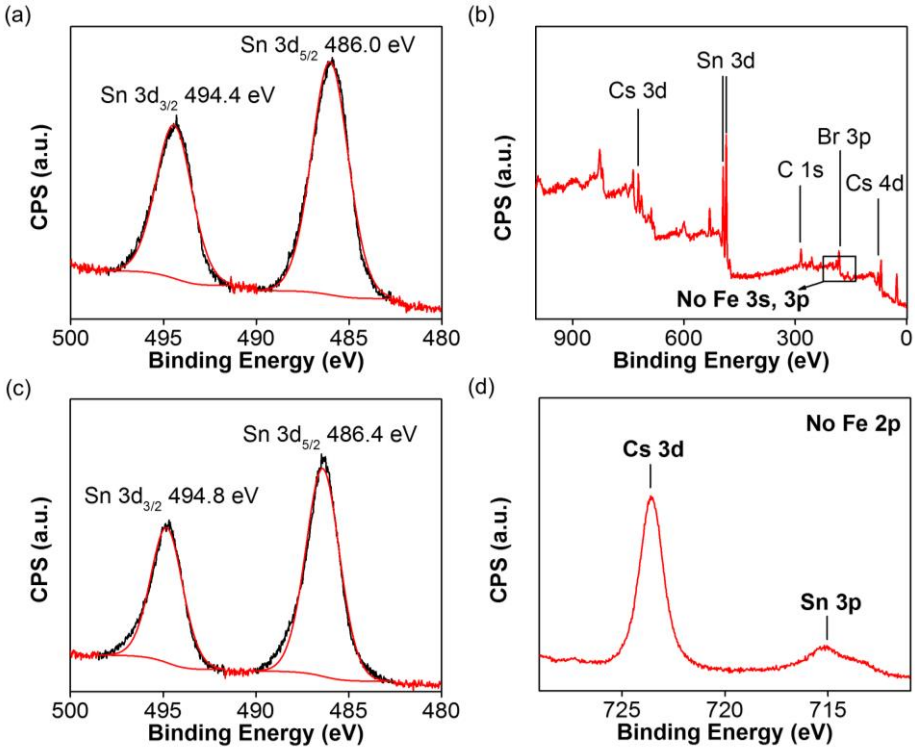

Figure S8. (a) Sn 3d XPS data for $CsSnBr_3$. (b) Survey spectrum of $CsSnBr_3$. (c) Sn 3d XPS data in $CsSnBr_3$ after being exposed to air. (d) no Fe was detected in the 2p range. Related to Figure 4.

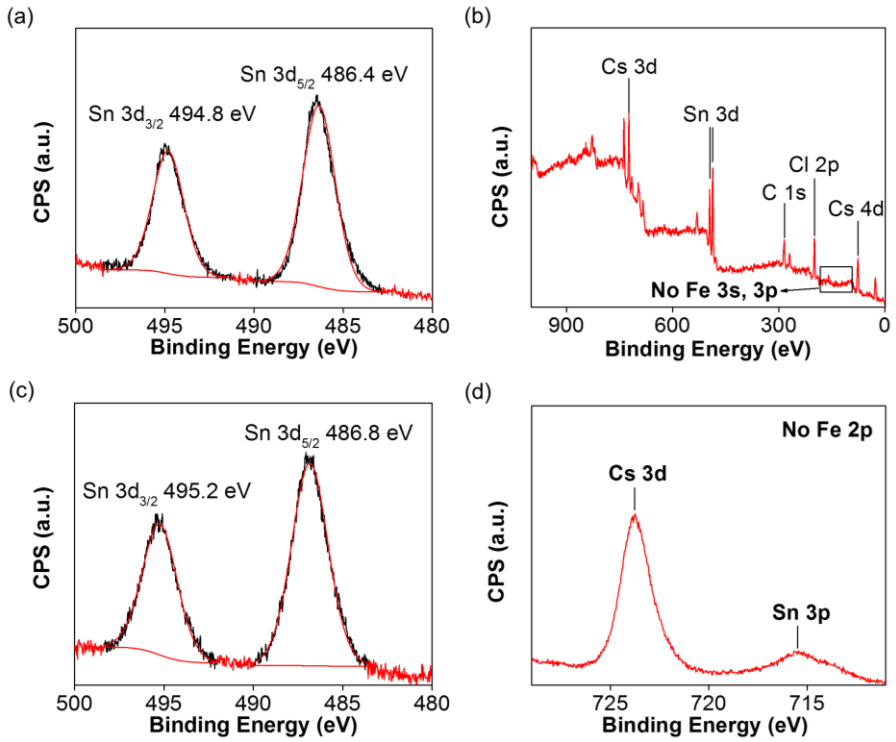

Figure S9. (a) Sn 3d XPS data for $CsSnCl_3$. (b) Survey spectrum of $CsSnCl_3$. (c) Sn 3d XPS data in $CsSnCl_3$ after being exposed to air. (d) no Fe was detected in the 2p range. Related to Figure 4.

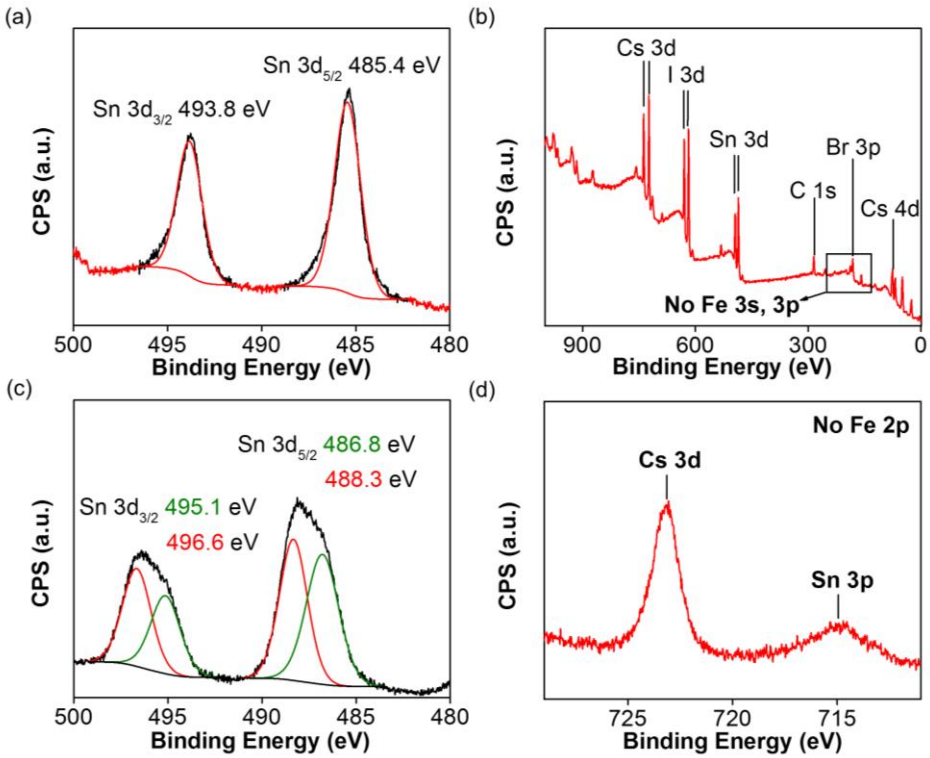

Figure S10. (a) Sn 3d XPS data for $CsSnBr_{1.5}I_{1.5}$. (b) Survey spectrum of $CsSnBr_{1.5}I_{1.5}$. (c) Sn 3d XPS data in $CsSnBr_{1.5}I_{1.5}$ after being exposed to air. (d) no Fe was detected in the 2p range. Related to Figure 4.

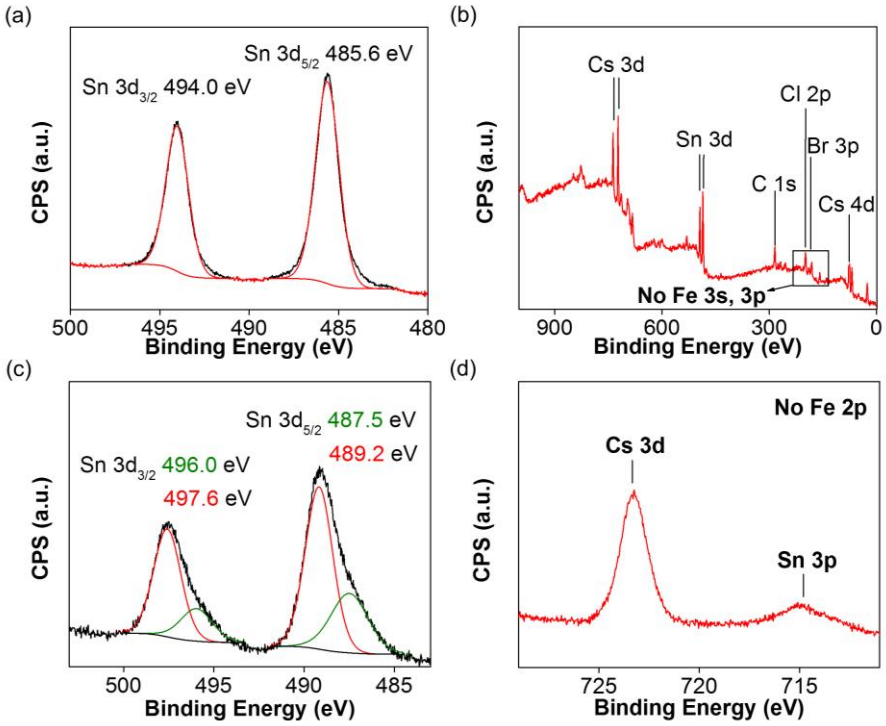

Figure S11. (a) Sn 3d XPS data for $CsSnBr_{1.5}Cl_{1.5}$. (b) Survey spectrum of $CsSnBr_{1.5}Cl_{1.5}$. (c) Sn 3d XPS data in $CsSnBr_{1.5}Cl_{1.5}$ after being exposed to air. (d) no Fe was detected in the 2p range. Related to Figure 4.

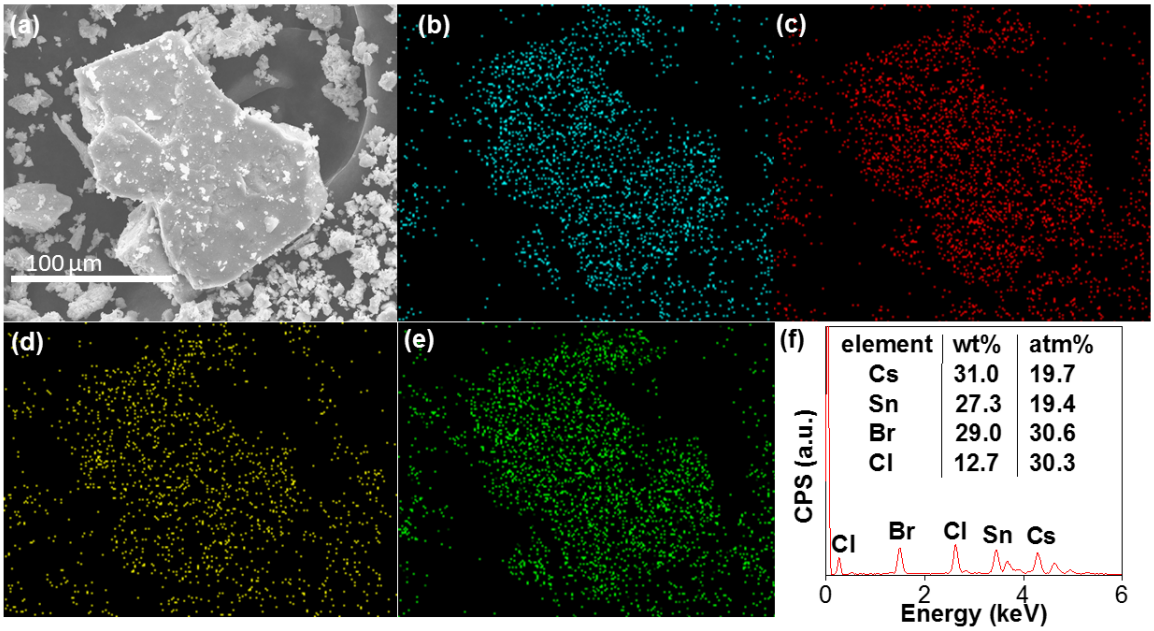

Figure S12. (a) SEM image of the mechanochemically synthesized $CsSnBr_{1.5}Cl_{1.5}$ perovskite, with the EDX analysis of the different elements (b) Cs (blue), (c) Sn (red), (d) Br (yellow), and (e) Cl (green), illustrating that all the elements are homogenously distributed throughout the solid particles. (f) The elemental composition as determined by EDX shows an approximately 1:1:1.5:1.5 molar ratio of Cs:Sn:Br:Cl atoms, which coincides with the chemical formula of $CsSnBr_{1.5}Cl_{1.5}$. It is worth noting that such precise stoichiometry is hard to achieve by solution-based methods. Related to Figure 4.

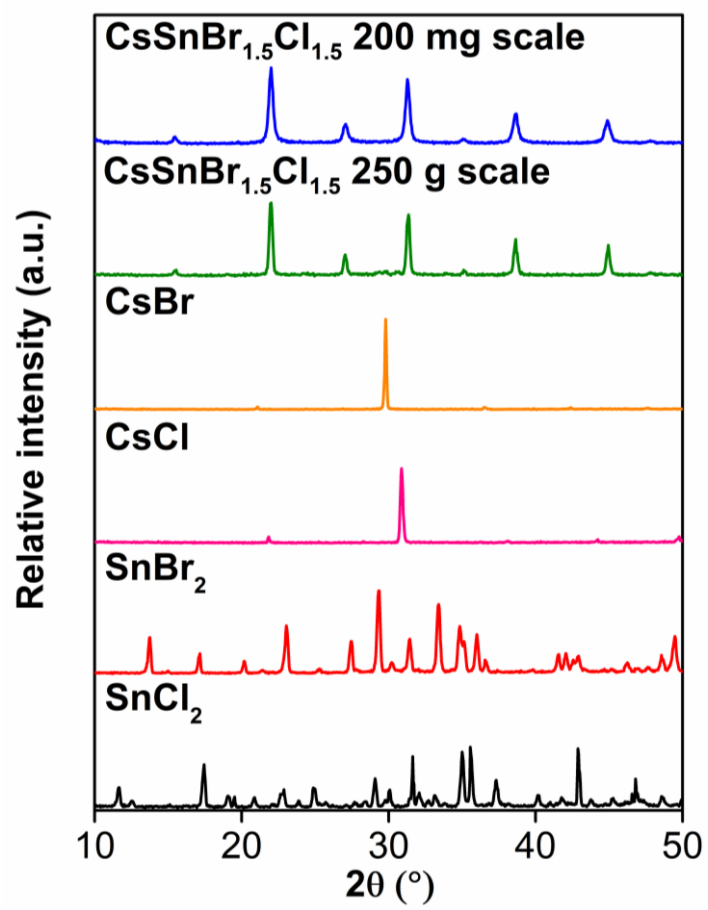

Figure S13. Comparison of the PXRD patterns of $CsSnBr_{1.5}Cl_{1.5}$ perovskite synthesized in 200 mg and 250 g scales, and the CsBr, CsCl, $SnBr_2$, and $SnCl_2$ precursors. The PXRD pattern of the 250 g scale synthesized product is almost indistinguishable from the small scale one and does not contain any precursor peaks. Related to Figures 1 and 4.

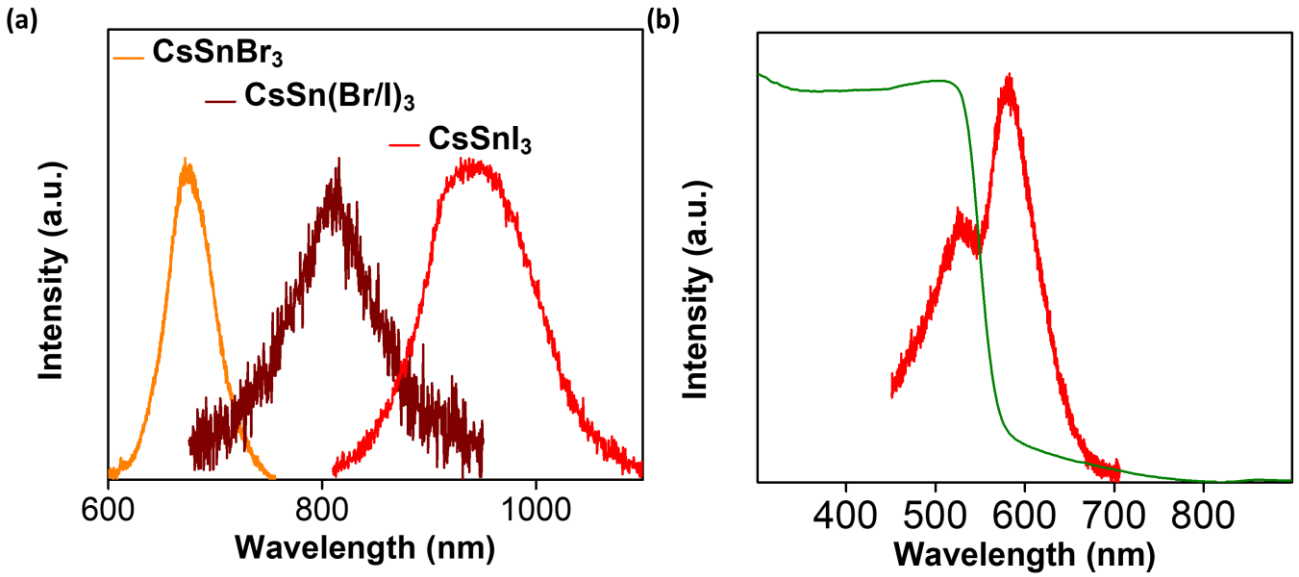

Figure S14. (a) PL data of spin-coated films of $CsSnBr_3$ (orange), $CsSnBr_{1.5}I_{1.5}$ (brown), and $CsSnI_3$ (red). (b) UV-vis DRS (green) and PL (red) data of mechanochemically synthesized $CsSnBr_{1.5}Cl_{1.5}$ powder. Related to Figures 4 and 6.

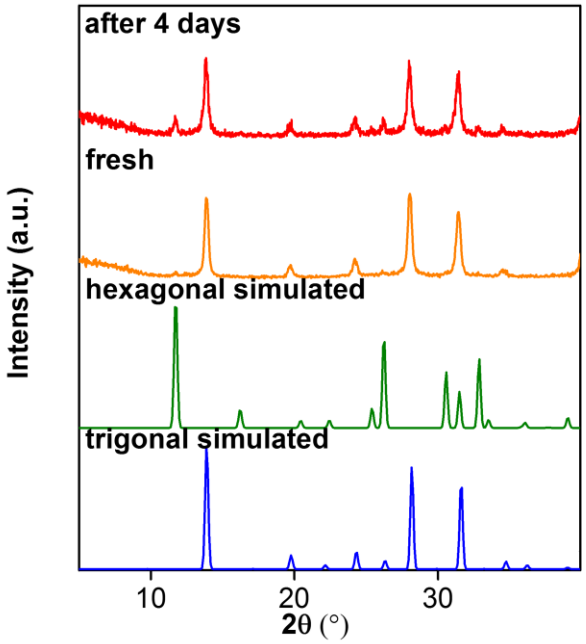

Figure S15. The PXRD patterns of $FAPbI_3$ showing phase transition within 4 days. Related to Figure 5.

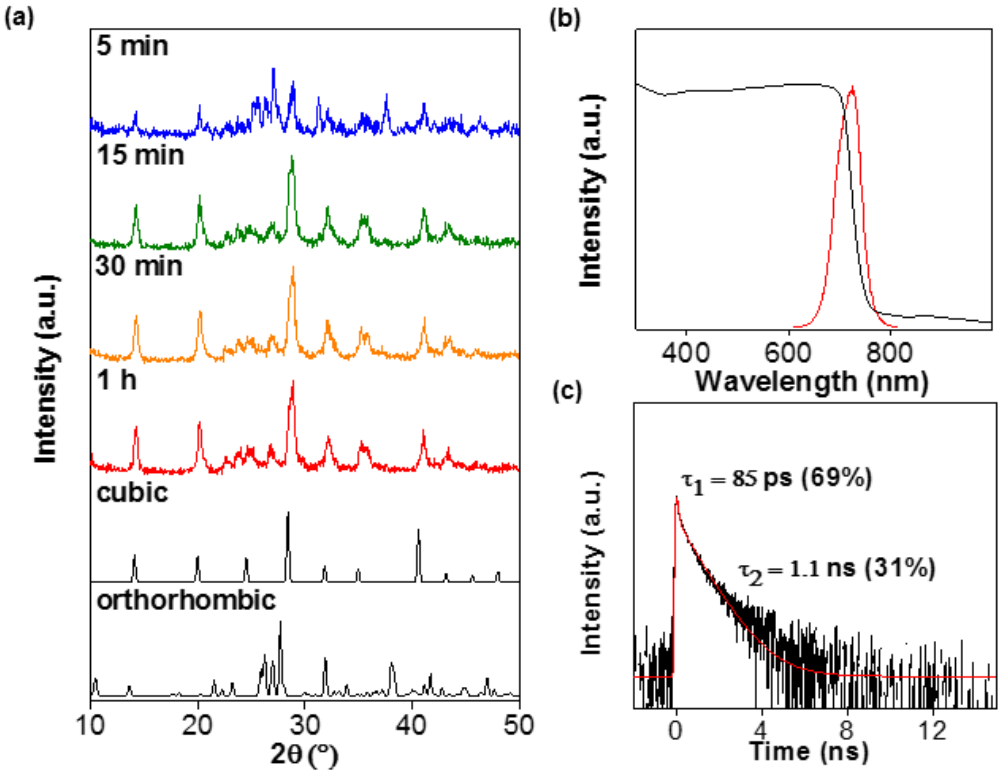

Figure S16. (a) The PXRD patterns of $CsPbI_3$ synthesized with different reaction durations and the simulated patterns for cubic and orthorhombic phases. (b) The UV-vis DRS spectrum (black) and the steady-state PL (red) of $CsPbI_3$. (c) The TRPL spectrum (black) of $CsPbI_3$. The plot was fitted biexponentially (red) to give a short-lived process with a lifetime of 85 ps (69%) and a longer process with a lifetime of 1.1 ns (31%). Related to Figures 5 and 6.

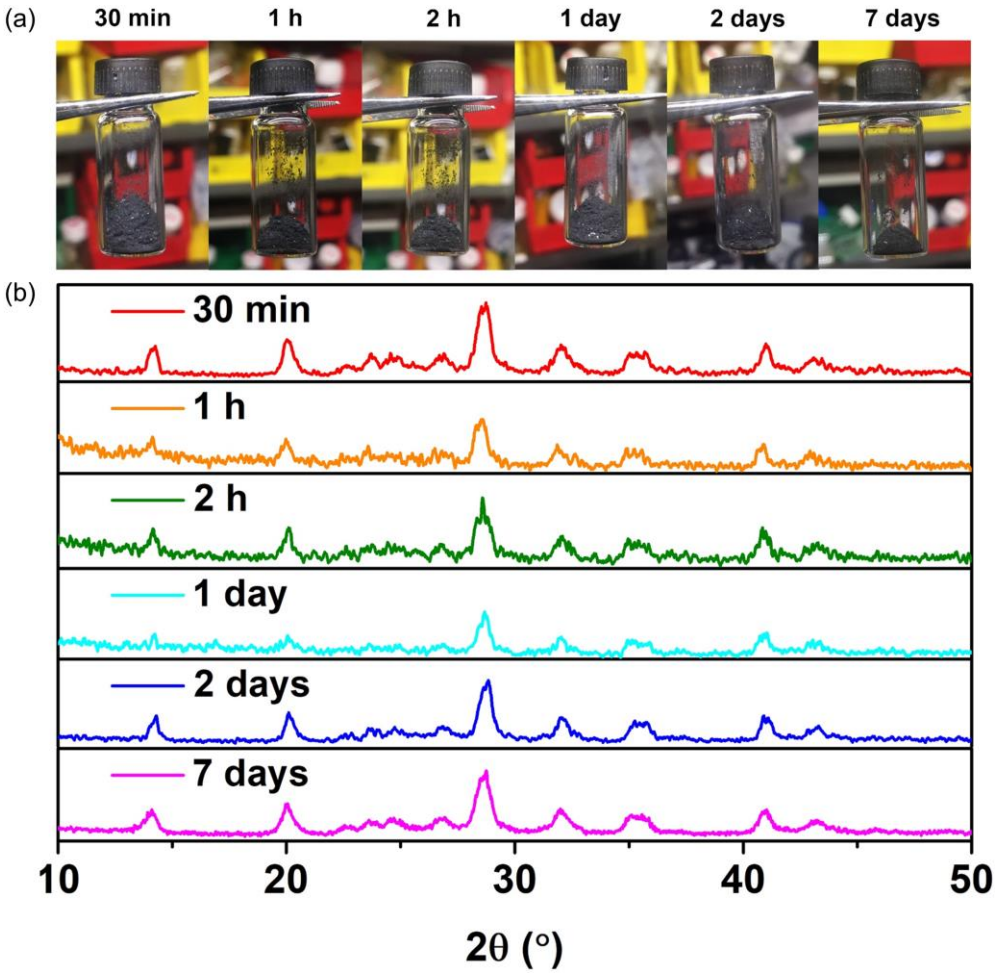

Figure S17. (a) Photographs of the black cubic $CsPbI_3$ synthesized by mechanochemical ball-milling and stored in a glovebox under < 0.5 ppm O_2 and water over seven days. (b) The PXRD pattern of the same mechanochemically prepared black cubic $CsPbI_3$ showing indefinite stability over the course of at least seven days, when stored in an inert atmosphere glovebox. Related to Figures 5 and 6.

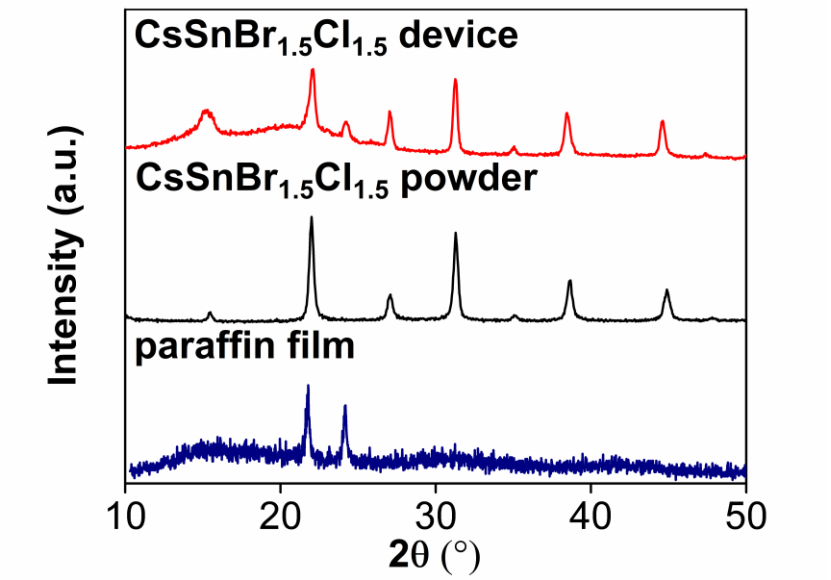

Figure S18. Comparison of the PXRD patterns of the $CsSnBr_{1.5}Cl_{1.5}$ perovskite device after gold electrode deposition with the as-synthesized powder. The peak position at 24° corresponds to the paraffin film that was used to seal the device in order to prevent the exposure to air. Based on the PXRD analysis, there is no significant structural change in the $CsSnBr_{1.5}Cl_{1.5}$ perovskite before and after the process of device fabrication. Related to Figure 7.

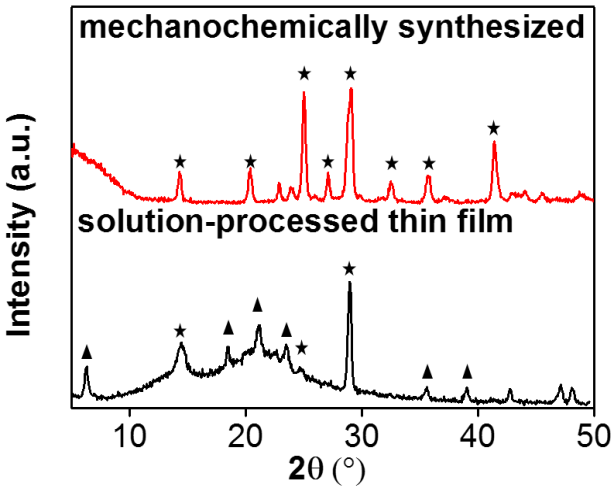

Figure S19. Comparison of the PXRD patterns of the $CsSnI_3$ perovskite that was synthesized mechanochemically (red line), with the sample prepared in solution by heating and spin-coating a thin film onto a glass substrate (black line). The product obtained by solution processing is not pure, since characteristic peaks belonging to the black orthorhombic phase and several other unidentifiable peaks were observed. Related to Figures 2 and 3.

Transparent Methods

Materials.

Cesium chloride (99%), cesium bromide (99.99%), cesium iodide (99.99%), lead iodide (99.999%) and formamidinium iodide (FAI, >99% anhydrous) were purchased from Sigma-Aldrich. Tin(II) chloride (99%) was purchased from Alfa Aesar. Tin(II) bromide (99.9%) was purchased from Sigma-Aldrich and tin(II) iodide (99.99%) was purchased from Strem Chemicals Corp. All the above chemicals were used directly without further purification and stored in a glovebox to minimize the exposure to oxygen. Notably, at the purity levels of the chemicals that we purchased, we did not observe any detectable impurities in the precursor salts that we used based on PXRD measurements (Figures 2e,f and S13). Consequently, no special procedures were necessary in handling the precursors as long as the newly purchased chemicals and the products were opened and handled exclusively in a well-maintained glovebox (O_2 levels < 1 ppm, water levels < 0.5 ppm). This has been further verified since we did not encounter unusual problems beyond the inherent air-, moisture-, and phase-instability of the perovskite products that we studied. Anhydrous dimethyl sulfoxide (DMSO, >99.9%) was purchased from Sigma-Aldrich and stored in a glovebox.

General mechanochemical synthesis procedure.

General procedure for mechanochemical synthesis: Stoichiometric equivalents of precursors (1:1 ratio between cation A^+ and B^{2+}) were mixed in a 25 mL stainless-steel milling jar (Form-Tech Scientific smart snap milling jar) equipped with a stainless-steel milling ball in a glovebox. The milling jar was installed into a shaker mill (Retsch MM400) and the milling was operated at a frequency of 30 Hz for 1 h. The milling jar was then taken into a glovebox, unsealed, and the resulting product was collected. Large scale syntheses were carried out using 250 mL stainless-steel milling jars on a Grinder BM4 planetary mill instead.

$CsSnI_3$: The general procedure was used with the following quantities: cesium iodide (77.9 mg, 0.30 mmol) and tin(II) iodide (112 mg, 0.30 mmol). The resulting product (150 mg, 79% yield) was collected as a black powder.

$CsSnBr_3$: The general procedure was used with the following quantities: cesium bromide (106 mg, 0.50 mmol) and tin(II) bromide (139 mg, 0.50 mmol). The resulting product (225 mg, 92% yield) was collected as a black powder.

$CsSnCl_3$: The general procedure was used with the following quantities: cesium chloride (84.2 mg, 0.50 mmol) and tin(II) chloride (94.8 mg, 0.50 mmol). The resulting product (145 mg, 81% yield) was collected as a yellow powder.

$CsSnBr_{1.5}Cl_{1.5}$: The general procedure was used with the following quantities: cesium bromide (53 mg, 0.25 mmol), tin(II) bromide (70 mg, 0.25 mmol), cesium chloride (42 mg, 0.25 mmol), and tin(II) chloride (47 mg, 0.25 mmol). The resulting product (169 mg, 79% yield) was collected as an orange powder.

$CsSnBr_{1.5}I_{1.5}$: The general procedure was used with the following quantities: cesium iodide (65 mg, 0.25 mmol), tin(II) iodide (93 mg, 0.25 mmol), cesium bromide (53 mg, 0.25 mmol), and tin(II) bromide (70 mg, 0.25 mmol). The resulting product (228 mg, 81% yield) was collected as a black powder.

$CsPbI_3$: The general procedure was used with the following quantities: cesium iodide (130 mg, 0.50 mmol) and lead(II) iodide (230 mg, 0.50 mmol). The mixed powder was ball-milled for 15 min resulting in the product (295 mg, 82% yield) as a black powder.

$FAPbI_3$: The general procedure was used with the following quantities: FAI (57 mg, 0.33 mmol), lead(II) iodide (153 mg, 0.33 mmol), and 0.10 mL of pentane added to assist the ball-milling (liquid assisted grinding, LAG). The mixture was milled for 15 min and the resulting product (168 mg, 80% yield) was collected as a black powder.

Large-scale synthesis:

$CsSnBr_3$ (25 g scale): Cesium bromide (10.6 g, 50 mmol) and tin(II) bromide (13.9 g, 50 mmol) were mixed in a 250 mL stainless-steel milling jar equipped with eight 4.0 g and fifteen 13.5 g stainless-steel milling balls (ball to reactant ratio = 2.35) in a glovebox. The milling jar was then installed into a Grinder BM4 planetary mill with four vessel holders and the milling was operated at 300 revolutions per minute (rpm, sun wheel speed) for cycles consisting of 3 min of continuous milling and a pause for 1 min, followed by a reverse in the rotation direction after each cycle, for a 3 hr total milling duration. The milling jar was then taken into a glovebox, unsealed, and the resulting black product (23.6 g, 94% yield) was collected.

$CsSnBr_{1.5}Cl_{1.5}$ (250 g scale): Cesium bromide (62.6 g, 0.29 mol), cesium chloride (49.6 g, 0.29 mol), tin(II) bromide (81.9 g, 0.29 mol), and tin(II) chloride (55.8 g, 0.29 mol) were mixed in a 250 mL stainless-steel milling jar equipped with fourteen 4.0 g and twenty 13.5 g stainless-steel balls (ball to reactant ratio = 1.30) in a glovebox. The milling jar was then installed into the same planetary mill and operated with the same milling cycles as the 25 g scale above, for a 2+2+2+2+2 = 10 hr total milling duration. Such interval milling was

performed to prevent overheating and reduce wear and tear on the planetary mill. The milling jar was then taken into a glovebox, unsealed, and the resulting black product (241 g, 96% yield) was collected.

Table S2. Synthetic details of the mechanochemically synthesized $CsSnX_3$ (mg scale). Related to Figures 1 and 4.

ABX_3	**Quantity of precursors**	**Product appearance**	**Yield**
$CsSnI_3$	CsI (77.9 mg, 0.30 mmol) SnI_2 (112 mg, 0.30 mmol)	black powder	150 mg, 79%
$CsSnBr_3$	CsBr (106 mg, 0.50 mmol) $SnBr_2$ (139 mg, 0.50 mmol)	black powder	225 mg, 92%
$CsSnCl_3$	CsCl (84.2 mg, 0.50 mmol) $SnCl_2$ (94.8 mg, 0.50 mmol)	yellow powder	145 mg, 81%
$CsSnBr_{1.5}Cl_{1.5}$	CsBr (53 mg, 0.25 mmol) $SnBr_2$ (70 mg, 0.25 mmol) CsCl (42 mg, 0.25 mmol) $SnCl_2$ (47 mg, 0.25 mmol)	orange powder	169 mg, 79%
$CsSnBr_{1.5}I_{1.5}$	CsI (65 mg, 0.25 mmol) SnI_2 (93 mg, 0.25 mmol) CsBr (53 mg, 0.25 mmol) $SnBr_2$ (70 mg, 0.25 mmol)	black powder	228 mg, 81%
$CsPbI_3$	CsI (130 mg, 0.50 mmol) PbI_2 (230 mg, 0.50 mmol)	black powder	295 mg, 82%
$FAPbI_3$	FAI (57 mg, 0.33 mmol) PbI_2 (153 mg, 0.33 mmol) 0.10 mL pentane for LAG	black powder	168 mg, 80%

Fabrication of solution processed samples

General procedure for the fabrication of a thin film sample: 10 µL of a 0.40 M precursor solution in DMSO was spin coated onto a quartz substrate at 4000 rpm for 30 s. In order to obtain high quality films, 100 µL of

toluene were dropped onto the substrate spinning at 4000 rpm for another 30 s. The coated substrate was then placed on a hot plate at 90 °C for 10 min.

Control experiments with heating only under solvent-free conditions

Stoichiometric equivalents of the precursors were mixed and sealed in a 25 mL reaction tube, heated at 325 °C under an argon atmosphere, cooled down to room temperature, and transferred into a glovebox. The reaction tube was unsealed and the resulting solid mixture was characterized by PXRD.

Fabrication of devices for photocurrent measurements

In a glovebox, the perovskite powder sample (300 mg) was placed between two stainless steel pellets in a hydraulic press and compressed with a force of 10^4 kg for 15 m. One of the resultant sample discs is shown in Figure 7(a). A typical sample disc is 2 mm in thickness. Each disc was then sealed in a 20 mL vial, placed into an air-tight Ziploc bag, and then transferred to the laboratory for the gold electrodes to be deposited.

Powder X-ray diffraction study

Measurements were performed on a Rigaku SmartLab X-ray diffractometer, fitted with a copper ($K_{\alpha1}$ (1.54059)/$K_{\alpha2}$ (1.54441) = 2) target X-ray tube set to 40 kV and 30 mA and a SC-70 scintillation detector. A medium resolution parallel-beam (PB) cross beam optics (CBO) unit was used with a 10 mm slit width. The powder samples were packed in airtight specimen holders (Bruker A100B33) in a glovebox. The respective PXRD patterns were obtained for 2θ angles from 4° to 50° at 0.04° per step.

Ultraviolet-visible diffuse reflectance spectroscopic (UV-vis DRS) study

UV-vis spectra were acquired using a Shimadzu UV-3600 UV-vis spectrometer with an integrating sphere (Shimadzu ISR-3100). Powder samples were sealed in quartz cuvettes.

X-ray photoelectron spectroscopic (XPS) study

XPS data were acquired using a Phoibos 100 spectrometer and a Mg X-ray source (SPECS, Germany) working at 12.5 kV equipped with dual Al/Mg anodes. Samples were prepared by coating a uniform layer of the materials on SPI double-sided adhesive carbon tape in a glovebox. The samples were then removed from the glovebox sealed in a vial and transferred to the laboratory for the spectrometer. Although there was a brief

exposure of each sample (< 5 s) when it was loaded into the spectrometer, the sample was then evacuated to a pressure below 10^{-8} mbar. Remarkably, no noticeable oxidation was observed despite the fact that XPS is a surface-sensitive technique. The carbon tape contains acrylate adhesives, so both C 1s and O 1s signals are present in the carbon tape itself. The XPS data were processed using the CasaXPS software. The spectra were calibrated internally according to the adventitious C 1s position at 284.6 eV.

Photoluminescence spectroscopic study

Measurements were carried out and ultrafast femtosecond optical spectroscopic methods were employed to measure the PL data and FWHM of the thin films. A Coherent Libra regenerative amplifier (50 fs, 1 kHz, 800 nm) seeded by a Coherent Vitesse Oscillator (100 fs, 80 MHz) were used as the pump laser sources. For pump wavelength tuning, the Coherent OPerA Solo optical parametric amplifier was used. Upon optically pumping the samples, the respective PL emissions were collected at a backscattering angle of 150° by a collimating lens pair and guided into an optical fiber that was coupled to a spectrometer (Acton, SpectraPro 2500i and SP2300) and detected by a charge coupled device (CCD; Princeton Instruments, Pixis 400B). Time-resolved PL (TRPL) was collected using an Optronis Optoscope streak camera system. For the spin-coated samples, 1:1 stoichiometric amounts of the respective salts were dissolved in DMF and spin-coated on 1x1 cm plasma-treated quartz substrates. The samples were then annealed at 373 K under a N_2 atmosphere. Due to the moisture sensitivity of the perovskites prepared, all samples were sealed into air-tight quartz cuvettes inside a glovebox. The optical measurements were performed at room temperature (295-298 K) under ambient pressures.

Photoelectrical study

Photoelectrical measurements were carried out using a Keithley 4200-SCS semiconductor characterization system with a coupled light source (Thorlabs Solis-445C) and a DC2200 driver. For each as-prepared perovskite pellet, the sample was removed from the vial, loaded, and then evacuated so that 200 nm thick gold electrodes could be deposited through thermal evaporation using shadow masks (active device area: 4000 µm × 200 µm = 8×10^{-7} m^2). The light source was operating at an intensity of 693.1 W/m^2. Detectivity is calculated using the formula below:

$$\textbf{Detectivity} = \textbf{Responsivity} \times \sqrt{\frac{\textbf{Device area}}{2e \times I_{dark}}}$$

Supplemental References

Askar, A.M., Karmakar, A., Bernard, G.M., Ha, M., Terskikh, V.V., Wiltshire, B.D., Patel, S., Fleet, J., Shankar, K., and Michaelis, V.K. (2018). Composition-Tunable Formamidinium Lead Mixed Halide Perovskites via Solvent-Free Mechanochemical Synthesis: Decoding the Pb Environments Using Solid-State NMR Spectroscopy. J Phys Chem Lett *9*, 2671-2677.

El Ajjouri, Y., Chirvony, V.S., Sessolo, M., Palazon, F., and Bolink, H.J. (2018a). Incorporation of potassium halides in the mechanosynthesis of inorganic perovskites: feasibility and limitations of ion-replacement and trap passivation. RSC Adv *8*, 41548-41551.

El Ajjouri, Y., Palazon, F., Sessolo, M., and Bolink, H.J. (2018b). Single-Source Vacuum Deposition of Mechanosynthesized Inorganic Halide Perovskites. Chem Mater *30*, 7423-7427.

Jana, A., Mittal, M., Singla, A., and Sapra, S. (2017). Solvent-free, mechanochemical syntheses of bulk trihalide perovskites and their nanoparticles. Chem Commun *53*, 3046-3049.

Karmakar, A., Askar, A.M., Bernard, G.M., Terskikh, V.V., Ha, M., Patel, S., Shankar, K., and Michaelis, V.K. (2018). Mechanochemical Synthesis of Methylammonium Lead Mixed–Halide Perovskites: Unraveling the Solid-Solution Behavior Using Solid-State NMR. Chem Mater *30*, 2309-2321.

Pal, P., Saha, S., Banik, A., Sarkar, A., and Biswas, K. (2018). All-Solid-State Mechanochemical Synthesis and Post-Synthetic Transformation of Inorganic Perovskite-type Halides. Chem Eur J *24*, 1811-1815.

Posudievsky, O.Y., Konoshchuk, N.V., Karbivskyy, V.L., Boiko, O.P., Koshechko, V.G., and Pokhodenko, V.D. (2017). Structural and Spectral Characteristics of Mechanochemically Prepared CsPbBr3. Theor Exp Chem *53*, 235-243.

Prochowicz, D., Yadav, P., Saliba, M., Kubicki, D.J., Tavakoli, M.M., Zakeeruddin, S.M., Lewiński, J., Emsley, L., and Grätzel, M. (2018). One-step mechanochemical incorporation of an insoluble cesium additive for high performance planar heterojunction solar cells. Nano Energy *49*, 523-528.

Prochowicz, D., Yadav, P., Saliba, M., Saski, M., Zakeeruddin, S.M., Lewiński, J., and Grätzel, M. (2017). Mechanosynthesis of pure phase mixed-cation MAxFA1−xPbI3 hybrid perovskites: photovoltaic performance and electrochemical properties. Sustainable Energy Fuels *1*, 689-693.

Protesescu, L., Yakunin, S., Nazarenko, O., Dirin, D.N., and Kovalenko, M.V. (2018). Low-Cost Synthesis of Highly Luminescent Colloidal Lead Halide Perovskite Nanocrystals by Wet Ball Milling. ACS Appl Nano Mater *1*, 1300-1308.

Sadhukhan, P., Kundu, S., Roy, A., Ray, A., Maji, P., Dutta, H., Pradhan, S.K., and Das, S. (2018). Solvent-Free Solid-State Synthesis of High Yield Mixed Halide Perovskites for Easily Tunable Composition and Band Gap. Cryst Growth Des *18*, 3428-3432.

Yun, S., Kirakosyan, A., Yoon, S.-G., and Choi, J. (2018). Scalable Synthesis of Exfoliated Organometal Halide Perovskite Nanocrystals by Ligand-Assisted Ball Milling. ACS Sustainable Chem Eng *6*, 3733-3738.